Investigation of a SPH-Based Sub-Cell Homogenization for PHWR Using a Multi-Cell Model

by

Thomas A. Ferguson

A thesis submitted to the
School of Graduate and Postdoctoral Studies in partial
fulfillment of the requirements for the degree of

Master of Applied Science

The Faculty of Energy Systems and Nucelar Science

Nuclear Engineering

University of Ontario Institute of Technology

Oshawa, Ontario, Canada

June 2018

THESIS EXAMINATION INFORMATION

Submitted by: **Thomas Ferguson**

Master of Applied Science in **Nuclear Engineering**

Thesis title:
Investigation of a SPH-Based Sub-Cell Homogenization for PHWR Using a Multi-Cell Model

An oral defense of this thesis took place on June 14, 2018 in front of the following examining committee:

Examining Committee:

Chair of Examining Committee	Dr. Jennifer McKellar
Research Supervisor	Dr. Eleodor Nichita
Examining Committee Member	Dr. Markus Piro
External Examiner	Dr. Anthony Waker, University of Ontario Institute of Technology

The above committee determined that the thesis is acceptable in form and content and that a satisfactory knowledge of the field covered by the thesis was demonstrated by the candidate during an oral examination. A signed copy of the Certificate of Approval is available from the School of Graduate and Postdoctoral Studies.

ABSTRACT

Superhomogenization (SPH) has gained interest in the industry as a possible method to overcome the inherent limitations of standard homogenization (SH) for full-nuclear-reactor-core neutronics calculations because its implementation does not require any changes to existing computer codes. Previous work found that single-cell SPH applied to Pressurized Heavy Water Reactors (PHWR) yields virtually no improvement compared to single-cell standard homogenization. This work attempts to improve those results by accounting for neutron leakage across cell boundaries by performing SPH-based homogenization using a 3×3 multi-cell model. The method is evaluated using a 5×5 lattice-cell model and comparing results for single-cell SH, multi-cell SH, single-cell SPH and multi-cell SPH. Results show that multi-cell SPH produces better results than single-cell SPH and multi-cell SH produces better results than single-cell SH. However, multi-cell SPH offers no improvement compared to multi-cell SH, just as single-cell SPH offers no improvement over single-cell SH.

Keywords: Applied Reactor Physics; Superhomogenization; SPH Factors; PHWR

AUTHOR'S DECLARATION

I hereby declare that this thesis consists of original work of which I have authored. This is a true copy of the thesis, including any required final revisions, as accepted by my examiners.

I authorize the University of Ontario Institute of Technology to lend this thesis to other institutions or individuals for the purpose of scholarly research. I further authorize University of Ontario Institute of Technology to reproduce this thesis by photocopying or by other means, in total or in part, at the request of other institutions or individuals for the purpose of scholarly research. I understand that my thesis will be made electronically available to the public.

_____ Thomas Ferguson

STATEMENT OF CONTRIBUTIONS

I hereby certify that I am the sole author of this thesis and that no part of this thesis has been published or submitted for publication. I have used standard referencing practices to acknowledge ideas, research techniques, or other materials that belong to others. Furthermore, I hereby certify that I am the sole source of the creative works and/or inventive knowledge described in this thesis.

ACKNOWLEDGEMENTS

I would sincerely like to thank my supervisor, Dr. Eleodor Nichita, for his encouragement, motivation and insight, which were very helpful during this work, especially with learning how to use the necessary computational tools.

I would also like to thank my family for all their encouragement and support throughout the whole process.

This work was supported in part by a joint grant from the Natural Sciences and Engineering Research Council of Canada and the University Network of Excellence in Nuclear Engineering.

TABLE OF CONTENTS

LIST OF TABLES

Chapter 2

Chapter 4

Chapter 5

Chapter 6

LIST OF FIGURES

Chapter 1

Chapter 2

Chapter 3

Chapter 4

Chapter 5

LIST OF ABBREVIATIONS AND SYMBOLS

BWR	Boiling Water Reactor
CP	Collision Probability
D	Diffusion Coefficient
D_2O	Heavy Water
E	Energy
FR	Fission Rate
He	Helium gas
J	Neutron Current
k_{eff}	Multiplication Eigenvalue
LWR	Pressurized Light Water Reactor
MC	Multi-Cell
MWd/t(U)	Mega watt days per metric ton of uranium fuel
n	Neutron density
p	Collision probability
PHWR	Pressurized Heavy Water Reactor
Q	Neutron source term
r	Spatial coordinate
RR	Reaction Rate
s	Neutron trajectory characteristic
SC	Single-Cell
SH	Standard Homogenization
SPH	Superhomogenization
t	time
UO_2	Uranium Dioxide
V	Volume
WIMS	Winfrith Improved Multi-group Scheme
WLUP	WIMS Library Update Project
μ	SPH equivalence factor
ν	Average number of neutrons produced per fission
Σ_a	Macroscopic absorption cross-section
Σ_f	Macroscopic fission cross-section
Σ_s	Macroscopic fission cross-section
υ	Neutron speed
ϕ	Transport neutron flux
χ	Fission neutron energy spectrum
ψ	Diffusion integrated neutron flux
Ω	Neutron solid angle

Chapter 1: Introduction

When designing a nuclear reactor, the main objective is to be able to control the neutron-induced fission chain reaction. Consequently, it is necessary to have an accurate description of the neutron interactions within the core. Reactor physics is the study of interactions of neutrons with matter (specific nuclides) inside a nuclear reactor. The interactions of neutrons with specific nuclides depend on neutron energy and on material properties, characterized by neutronic-reaction *macroscopic cross-sections*. The fission rate depends on the fission macroscopic cross section and on the distribution of the neutron flux within the reactor, which can be determined by solving the neutron transport equation. A statistical mechanical approach has been used to derive the neutron transport equation.

For most designs of nuclear reactor cores, the fuel is contained within fuel rods. These fuel rods are grouped together, for a Light Water Reactor (LWR), these groupings are in a rectangular arrangement known as a fuel assembly. For Pressurized Heavy Water Reactors (PHWRs), the reactors investigated in this thesis, the fuel rods are grouped in an annulus arrangement known as a fuel bundle. A typical 37 element PHWR fuel bundle, pressure tube, and calandria tube used at the Bruce Nuclear Generation Station is depicted in Figure 1.1 below.

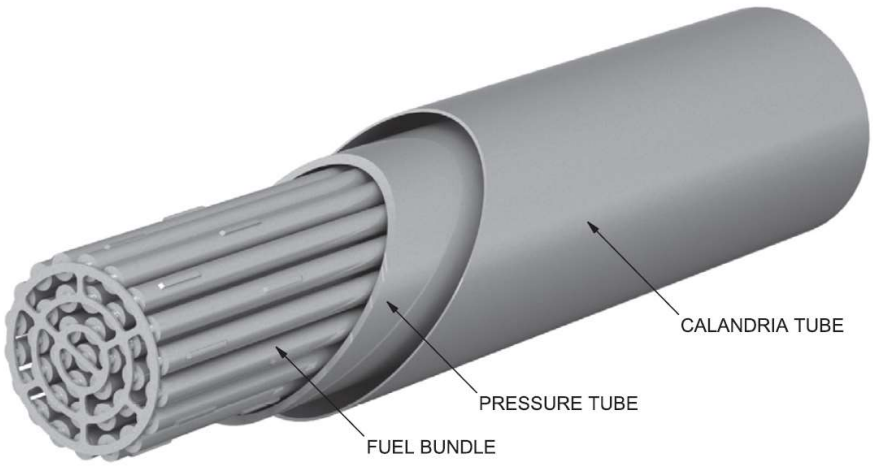

Figure 1.1: The configuration of the PHWR fuel channel including the fuel bundle, pressure tube, and calandria tube (Piro et al., 2017).

The reactor then consists of a periodic array of either fuel assemblies or fuel bundles. If an axial cross-section was taken through the core a two-dimensional periodic array is observed. The periodic array consists of a repeated geometric unit that contains the fuel, coolant, and surrounding moderator. This two-dimensional geometric unit is referred to as a lattice cell. In the case of PHWR the lattice cell contains the fuel bundle.

Reactor cores consist of multiple materials, and the cross-sections drastically change both spatially and over the spectrum of neutron energies. Such large energy and space variations in macroscopic cross-section values make it impossible to obtain analytical solutions for the transport equation and make numerical solutions computationally expensive. To be useful for production calculations which need to be computationally inexpensive, full reactor core calculations are generally performed in two steps: a lattice step and a core step. The first step is the lattice calculation, whereby the neutron flux is obtained as the solution to the neutron transport equation solved for a model representing

a single unit cell, or fuel assembly. Once the flux distribution in the lattice cell is found, the macroscopic cross-sections calculation is weighted with the neutron flux and averaged over the lattice cell and over energy to generate homogenized and energy condensed cross-sections and diffusion coefficients. The averaged parameters are subsequently used in an approximation of the transport equation, known as the diffusion equation, to complete a full-core calculation, the second step of the whole procedure. The solution to the diffusion equation provides the reactor flux distribution in the entire core, which is used for calculating the power distribution in the reactor. Because most of the lattice heterogeneity occurs in the axial plane, lattice calculations and subsequent homogenization are usually performed for two-dimensional lattice cells located at different axial positions. The corresponding homogenized cross-sections have a relatively smooth axial variation and do not require any special treatment.

The transport equation for neutrons will be reviewed in the following section (1.1) along with the method used for solving the equation in this thesis. An overview of the diffusion theory and how it applies to the transport equation will be discussed in section 1.2, followed by an overview of standard homogenization in the concluding section (1.3).

1.1. The Neutron Transport Equation

1.1.1. Deriving the Transport Equation

When discussing the behaviour of neutrons interacting with matter, it is not practical to analyze each particle individually due to the large population of particles. Instead we deal with a neutron density distribution in phase space (position and velocity vectors) and as a function of time, which requires a statistical mechanical approach. The transport

equation is used to describe the neutron density distribution in a closed domain, in either transient or steady state conditions. The equation is derived from the conservation of particles and is thus a neutron balance equation.

It is convenient to use the neutron angular flux as the unknown function in the transport equation. The neutron angular flux is related to the neutron density by the following expression:

$$\phi(\boldsymbol{r}, v, \boldsymbol{\Omega}, t) \equiv vn(\boldsymbol{r}, v, \boldsymbol{\Omega}, t) \tag{1.1}$$

Each particle is moving in six-dimensional phase space consisting of three spatial dimensions ($\boldsymbol{r} = x\boldsymbol{i} + y\boldsymbol{j} + z\boldsymbol{k}$), and three velocity dimensions, which consists of the module of velocity, ($v = |\boldsymbol{v}|$), and the direction given by a unit vector, $\boldsymbol{\Omega} = \frac{\boldsymbol{v}}{|\boldsymbol{v}|}$. The neutron density is then a distribution with respect to $\boldsymbol{r}, v, \boldsymbol{\Omega}$, and a function with respect to time, t.

To simplify the description of the neutron behavior in a reactor, four assumptions are made:

1. Relativistic effects can be neglected.
2. Neutron-neutron interactions can be ignored.
3. Neutrons travel in straight lines between interactions
4. Materials are isotropic.

These assumptions are valid because the kinetic energy of neutrons in a reactor are generally much smaller then required for relativistic effects to be noticeable, the neutron density in a reactor is much smaller then the density of nuclei, and neutron-nucleus

collisions are independent of the direction of the incident neutron. Due to the absence of neutron-neutron interactions, the transport equation becomes a linear variant of the Boltzmann equation. Since the neutron transport equation expresses the neutron balance, we derive it by setting the rate of change of the neutrons equal to the difference of the neutron production rate and the neutron loss rate in a control volume, V, defined by a surface, S for particles traveling at a speed within dv, with direction within $d^2\Omega$ (Herbert, 2009). The rate of change for a finite volume can be expressed by the following:

$$\dot{n}(v, \boldsymbol{\Omega}, t) = \lim_{t \to 0} \frac{1}{\Delta t} \int_V [n(\boldsymbol{r}, v, \boldsymbol{\Omega}, t + \Delta t) - n(\boldsymbol{r}, v, \boldsymbol{\Omega}, t)] d^3 r dv d^2\Omega \tag{1.2}$$

The loss rate of neutrons in the same volume is determined by the loss of neutrons streaming (or leaking) out of the volume, and by the rate of neutrons in the control volume with a velocity within dv, and a direction within $d^2\Omega$, colliding with a nucleus. The rate at which neutron stream out is given by Eq. (1.3).

$$L = \int_S (\boldsymbol{\Omega} \cdot \boldsymbol{N}) \phi(\boldsymbol{r}, v, \boldsymbol{\Omega}, t) d^2 r dv d^2\Omega \tag{1.3}$$

Where $\boldsymbol{N}$ is the normal vector of surface S, pointing outward from the volume element. Applying Divergence Theorem to Eq. (1.3) and using the identity $\boldsymbol{\nabla} \cdot \boldsymbol{\Omega} f(\boldsymbol{r}) = \boldsymbol{\Omega} \cdot \boldsymbol{\nabla} \mathrm{f}(\mathbf{r})$ gives the following:

$$L = \int_V \boldsymbol{\Omega} \cdot \boldsymbol{\nabla} \phi(\boldsymbol{r}, v, \boldsymbol{\Omega}, t) d^3 r dv d^2\Omega \Delta t \tag{1.4}$$

The rate at which neutrons collide with nuclei is given by Eq. (1.5).

$$C = \int_V \Sigma(\boldsymbol{r}, v) [v \cdot n(\boldsymbol{r}, v, \boldsymbol{\Omega}, t)] d^3 r dv d^2\Omega \tag{1.5}$$

Where $\Sigma(\boldsymbol{r}, v)$, is the total macroscopic cross-section at position $\boldsymbol{r}$. The production rate of neutrons is given in Eq. (1.6).

$$P = \int_V Q(\boldsymbol{r}, \upsilon, \boldsymbol{\Omega}, t) d^3 r d\upsilon d^2\Omega \tag{1.6}$$

The source density is expressed as $Q(\boldsymbol{r}, \upsilon, \boldsymbol{\Omega}, t)$ in the above equation. The particle balance equation can then be expressed by the following:

$$\dot{n} = -L - C + P \tag{1.7}$$

Since the control volume is arbitrary, and every term in Eq. (1.7) is expressed in terms of a three-dimensional volume integral, the integrands of all the terms in Eq. (1.7) must satisfy the same equality. As a result, Eq. (1.7) can be rewritten to give Eq. (1.8).

$$\dot{n}(\boldsymbol{r}, \upsilon, \boldsymbol{\Omega}, t) = -\boldsymbol{\Omega} \cdot \boldsymbol{\nabla}\phi(\boldsymbol{r}, \upsilon, \boldsymbol{\Omega}, t) - \Sigma(\boldsymbol{r}, \upsilon)[\upsilon \cdot n(\boldsymbol{r}, V_n, \boldsymbol{\Omega}, t)] + Q(\boldsymbol{r}, \upsilon, \boldsymbol{\Omega}, t) \tag{1.8}$$

Substituting the angular flux based on Eq. (1.1), the neutron transport equation is given as:

$$\frac{1}{\upsilon}\frac{\partial}{\partial t}\phi(\boldsymbol{r}, \upsilon, \boldsymbol{\Omega}, t) + \boldsymbol{\Omega} \cdot \boldsymbol{\nabla}\phi(\boldsymbol{r}, \upsilon, \boldsymbol{\Omega}, t) + \Sigma(\boldsymbol{r}, \upsilon)\phi(\boldsymbol{r}, \upsilon, \boldsymbol{\Omega}, t) \; = Q(\boldsymbol{r}, \upsilon, \boldsymbol{\Omega}, t) \tag{1.9}$$

The transport equation is often expressed in terms of energy, E, and will be for the rest of this thesis, instead of the neutron velocity, υ. Since neutron flux is a distribution the change of variables requires Eq. (1.10) to be satisfied.

$$|\phi(\boldsymbol{r}, \upsilon, \boldsymbol{\Omega}, t) d\upsilon| = |\phi(\boldsymbol{r}, E, \boldsymbol{\Omega}, t) dE| \tag{1.10}$$

The relationship between energy and neutron speed is given by the classical formula for kinetic energy as follows.

$$E = \frac{1}{2} m\upsilon^2 \; and \; dE = m\upsilon d\upsilon \tag{1.11}$$

Then Eq. (1.10) can be rewritten to give the relationship between $\phi(\boldsymbol{r}, \upsilon, \boldsymbol{\Omega}, t)$ and $\phi(\boldsymbol{r}, E, \boldsymbol{\Omega}, t)$.

$$\phi(\boldsymbol{r}, E, \boldsymbol{\Omega}, t) = \frac{1}{m\upsilon}\phi(\boldsymbol{r}, \upsilon, \boldsymbol{\Omega}, t) \tag{1.12}$$

Under steady-state conditions, the rate of change of the particle population is zero and Eq. (1.9) can then be expressed as:

$$\boldsymbol{\Omega} \cdot \boldsymbol{\nabla}\phi(\boldsymbol{r}, E, \boldsymbol{\Omega}) + \Sigma(\boldsymbol{r}, E)\phi(\boldsymbol{r}, E, \boldsymbol{\Omega}) = Q(\boldsymbol{r}, E, \boldsymbol{\Omega}) \tag{1.13}$$

The work presented in this thesis will always be under steady-state conditions and all further derivations will be presented as such. The loss of neutrons by collision can be expressed in terms of rate of neutrons being absorbed and the rate of neutrons scattering out of the energy range dE and direction $d^2\Omega$. The loss of neutrons from absorption and loss of neutrons from scattering is shown in Eq. (1.14).

$$\Sigma(\boldsymbol{r}, E)\phi(\boldsymbol{r}, E, \boldsymbol{\Omega}) = \Sigma_a(\boldsymbol{r}, E)\phi(\boldsymbol{r}, E, \boldsymbol{\Omega}) + \int_0^\infty dE' \int_{4\pi} d^2\Omega' \Sigma_s(\boldsymbol{r}, E \to E', \boldsymbol{\Omega} \to \boldsymbol{\Omega}')\phi(\boldsymbol{r}, E, \boldsymbol{\Omega}) \tag{1.14}$$

Where $\Sigma_a(\boldsymbol{r}, E)$ is the macroscopic absorption cross-section, and $\Sigma_s(\boldsymbol{r}, E \to E', \boldsymbol{\Omega} \to \boldsymbol{\Omega}')$ is the macroscopic differential scattering cross-section. The integrals are over all possible resulting angles and energies after scattering. The source of neutrons can be expressed in terms of neutrons scattering into the control volume from other directions and energies and for a multiplying medium, the addition of neutrons produced from fission. The source term or the gain from scattering and the production from fission is described in Eq. (1.15).

$$Q(\boldsymbol{r}, E, \boldsymbol{\Omega}) = \int_0^\infty dE' \int_{4\pi} d^2\Omega' \Sigma_s(\boldsymbol{r}, E' \to E, \boldsymbol{\Omega}' \to \boldsymbol{\Omega})\phi(\boldsymbol{r}, E', \boldsymbol{\Omega}') +$$

$$\frac{1}{4\pi K_{eff}} \sum_{j=i}^{J} \chi_j(E) \int_0^\infty dE' \, \nu\Sigma_{f,j}(\boldsymbol{r}, E')\phi(\boldsymbol{r}, E') \tag{1.15}$$

The macroscopic cross-section for neutrons scattering into the control volume is $\Sigma_s(\boldsymbol{r}, E' \rightarrow E, \boldsymbol{\Omega}' \rightarrow \boldsymbol{\Omega})$. In Eq. (1.15), j is the total number of fissionable isotopes, $\nu \Sigma_{f,j}(\boldsymbol{r}, E')$ is the number of neutrons produced per fission times the macroscopic cross-section for fission of the j^{th} fissionable isotope and K_{eff} is the effective multiplication factor, which is used to maintain a steady state, and ensure a solution. The probability for a neutron to be emitted from the fission of the j^{th} fissionable isotope with energy E is given by the fission spectrum $\chi_j(E)$, and is normalized by Eq. (1.16).

$$\int_0^\infty \chi_j(E) dE = 1 \tag{1.16}$$

Substituting Eq. (1.14) and (1.15) into Eq. (1.13) gives the integro-differential form of the transport equation:

$$\boldsymbol{\Omega} \cdot \boldsymbol{\nabla}\phi(\boldsymbol{r}, E, \boldsymbol{\Omega}) + \Sigma_a(\boldsymbol{r}, E)\phi(\boldsymbol{r}, E, \boldsymbol{\Omega}) + \int_0^\infty dE' \int_{4\pi} d^2\Omega' \Sigma_s(\boldsymbol{r}, E \rightarrow E', \boldsymbol{\Omega} \rightarrow \boldsymbol{\Omega}')\phi(\boldsymbol{r}, E, \boldsymbol{\Omega}) = \int_0^\infty dE' \int_{4\pi} d^2\Omega' \Sigma_s(\boldsymbol{r}, E' \rightarrow E, \boldsymbol{\Omega}' \rightarrow \boldsymbol{\Omega})\phi(\boldsymbol{r}, E', \boldsymbol{\Omega}') + \frac{1}{4\pi K_{eff}} \sum_{j=i}^{J} \chi_j(E) \int_0^\infty dE' \nu\Sigma_{f,j}(\boldsymbol{r}, E')\phi(\boldsymbol{r}, E') \tag{1.17}$$

To generating numerical solutions for the transport equation the energy variable is first discretized into multiple groups. This is done by dividing the entire energy domain into G groups, indexed by g. All the energy dependent properties are averaged over the group. Eq. (1.17) can be expressed as multi-group neutron balance equation as shown in Eq. (1.18).

$$\boldsymbol{\Omega} \cdot \boldsymbol{\nabla}\phi_g(\boldsymbol{r}, \boldsymbol{\Omega}) + \Sigma_{a,g}(\boldsymbol{r})\phi_g(\boldsymbol{r}, \boldsymbol{\Omega}) + \sum_{g'} \int_{4\pi} d^2\Omega' \Sigma_{g \rightarrow g'}(\boldsymbol{r}, \boldsymbol{\Omega} \rightarrow \boldsymbol{\Omega}')\phi_g(\boldsymbol{r}, \boldsymbol{\Omega}) =$$

$$\sum_{g'} \int_{4\pi} d^2\Omega' \Sigma_{g' \to g}(\boldsymbol{r}, \boldsymbol{\Omega}' \to \boldsymbol{\Omega}) \phi_{g'}(\boldsymbol{r}, \boldsymbol{\Omega}') + \frac{1}{4\pi K_{eff}} \sum_{j=i}^{J} \chi_{jg} \sum_{g} \nu\Sigma_{f,j,g}(\boldsymbol{r}) \phi_g(\boldsymbol{r})$$

(1.18)

The neutron transport equation given in Eq. (1.18), being an integro-differential equation of 5 independent variables (three spatial variables and two angular variables) and does not have simple analytical or numerical solutions. However, there are a multitude of different methods for solving it. Many of the solutions necessitate simplification of Eq. (1.18) that comes from the transport equation being expressed in other forms. A common method for solving the transport equation, and the method used in this study, known as the Collision Probability method utilizes the integral form of the neutron transport equation. The integral transport equation is obtained by integrating the angular flux along its characteristic line for a given source density (Sanchez & McCormick, 1981). The characteristic defines the path a neutron travels between points $\boldsymbol{r}$ and $\boldsymbol{r}'$ in the absence of any interaction. If a neutron travels in a straight line between $\boldsymbol{r}$ and $\boldsymbol{r}'$ in the direction $\boldsymbol{\Omega}$, then the following relationship can be expressed:

$$\boldsymbol{r} = \boldsymbol{r}' + s\boldsymbol{\Omega} \tag{1.19}$$

Where s is the magnitude of the vector $\boldsymbol{r} - \boldsymbol{r}'$. The derivative along the path can then be described as:

$$\frac{d}{ds} = \frac{\partial \boldsymbol{r}'}{\partial s} \cdot \boldsymbol{\nabla}_{\boldsymbol{r}'} \tag{1.20}$$

Using Eq. (1.20) we can then rewrite Eq. (1.13) as the following:

$$\left[\frac{\mathrm{d}}{\mathrm{ds}} - \Sigma(\boldsymbol{r}, E)\right] \phi(\boldsymbol{r}, E, \boldsymbol{\Omega}) = -Q(\boldsymbol{r}, E, \boldsymbol{\Omega}) \tag{1.21}$$

Where $Q(\boldsymbol{r}, E, \boldsymbol{\Omega})$ is the source density as described in Eq. (1.15). The above equation is now a first order ordinary differential equation, which can be solved by introducing an integration factor, $e^{-\tau(s,E)}$. The optical path is expressed as τ in the integration factor and is defined as a function of the macroscopic cross section.

$$\tau(s, E) = \int_0^S ds' \Sigma(\boldsymbol{r} - s'\boldsymbol{\Omega}, \mathrm{E}) \tag{1.22}$$

The solution of Eq. (1.21) is then expressed as:

$$\phi(\boldsymbol{r}, E, \boldsymbol{\Omega}) = \phi(\boldsymbol{r} - b\boldsymbol{\Omega}, E, \boldsymbol{\Omega}) e^{-\tau(b,E)} + \int_0^S ds e^{-\tau(s,E)} Q\,(\boldsymbol{r} - s\boldsymbol{\Omega}, E, \boldsymbol{\Omega}) \tag{1.23}$$

The above equation is the integral neutron transport equation for a finite domain where $\phi(\boldsymbol{r} - b\boldsymbol{\Omega}, E, \boldsymbol{\Omega})$ is determined according to the boundary conditions. The integral neutron transport equation can then also be expressed in its multigroup formulization shown in Eq. (1.24).

$$\phi_g(\boldsymbol{r}, \boldsymbol{\Omega}) = \phi_g(\boldsymbol{r} - b\boldsymbol{\Omega}, \boldsymbol{\Omega}) e^{-\tau_g(b)} + \int_0^S ds e^{-\tau_g(s)} Q_g\,(\boldsymbol{r} - s\boldsymbol{\Omega}, \boldsymbol{\Omega}) \tag{1.24}$$

1.1.2. Collision Probability Method

As mentioned in the previous section, there are a multitude of methods for solving the neutron transport equation. In this section a brief overview of the collision probability method will be presented, since it is the method used to solve the transport equation in this thesis. The method utilizes the integration transport equation (Sanchez & McCormick, 1981), shown in Eq. (1.23). The multigroup integration transport equation for a reactor with void boundary conditions (there is no incoming neutron current at the boundaries), the fist term in Eq. (1.24) goes to zero and can be rewritten as shown in Eq. (1.25).

$$\phi_g(\boldsymbol{r},\boldsymbol{\Omega}) = \int_0^s ds e^{-\tau_g(s)} Q_g(\boldsymbol{r}-s\boldsymbol{\Omega},\boldsymbol{\Omega}) \tag{1.25}$$

Since reaction rates are independent on the direction of the incident neutron flux, it is more useful to define the group integral flux as:

$$\phi_g(\boldsymbol{r}) = \int_\Omega d^2\Omega \phi_g(\boldsymbol{r},\boldsymbol{\Omega}) \tag{1.26}$$

Applying Eq. (1.26) to (1.25), assuming the source to be isotropic, and introducing the change of variables $\boldsymbol{r'} = \boldsymbol{r} - s\boldsymbol{\Omega}$, and $d^3r' = s^2 d^2\Omega ds$ the following is obtained:

$$\phi_g(\boldsymbol{r}) = \frac{1}{4\pi}\int_0^s d^3r' \frac{e^{-\tau g(s)}}{s^2} Q_g(\boldsymbol{r'}) \tag{1.27}$$

The above equation represents a lattice of identical unit cells, which can be partitioned further into sub-cell regions V_i. Eq. (1.27) is then multiplied by $\Sigma_g(\boldsymbol{r})$ and integrated over each region V_i, to give Eq. (1.28).

$$\int_{V_j} d^3r \Sigma_g(\boldsymbol{r})\phi_g(\boldsymbol{r}) = \frac{1}{4\pi}\int_{V_j} d^3r \Sigma_g(\boldsymbol{r}) \sum_i Q_{i,g} \int_{V_i} d^3r' \frac{e^{-\tau g(s)}}{s^2} \tag{1.28}$$

$$Q_{i,g} = \sum_h \Sigma_{s,i,g\leftarrow h}\phi_{i,g} + \frac{1}{K_{eff}} Q_{i,g}^{fiss} \tag{1.29}$$

The fissions source term in Eq. (1.29) is given as:

$$Q_{i,g}^{fiss} = \sum_{j=1}^{J^{fiss}} \chi_{j,g} \sum_h \nu\Sigma_{f,j,h}\phi_{i,h} \tag{1.30}$$

Where j is the number fissionable isotopes, and $\chi_{j,g}$ is the fission spectrum of isotope j in energy group g. Eq. (1.28) can be simplified to Eq. (1.31).

$$V_j\Sigma_{j,g}\phi_{j,g} = \sum_i Q_{i,g} V_i P_{ij,g} \tag{1.31}$$

The collision probability (CP) is $P_{ij,g}$, and is the probability for a neutron born uniformly and isotopically in region V_i, to undergo its first collision in V_j. If the total cross section is constant and equal to the macroscopic constant in each region, the collision probabilities can then be defined as reduced CPs and are expressed as follows.

$$p_{ij,g} = \frac{P_{ij,g}}{\Sigma_{j,g}} = \frac{1}{4\pi V_i} \int_{V_i} d^3r' \int_{V_j} d^3r \frac{e^{-\tau_g(s)}}{s^2} \tag{1.32}$$

Collision probabilities have reciprocity and conservation properties such that the following relationships are obeyed:

$$p_{ij,g} V_i = p_{ji,g} V_j \tag{1.33}$$

$$\sum_j p_{ij,g} \Sigma_{j,g} = 1; \ \forall i \tag{1.34}$$

Using the reciprocity property, the expression for flux can be further simplified to give the following:

$$\phi_{i,g} = \sum_j p_{ij,g} \mathrm{Q}_{j,g} \tag{1.35}$$

The collision probability method is normally performed in the three following steps. The first step is applying a tracking process applied over the entire lattice geometry to give sufficiently large number of neutron trajectories. The second step is performing a numerical integration using the tracking data and macroscopic cross sections for each region to determine the collision probabilities. The final step is solving the integrated flux using Eq. (1.29) and (1.35) (Herbert, 2009).

1.2. Diffusion Equation

The diffusion equation approximates the transport equation by utilizing Fick's Law to give a simpler description of the neutron current. Fick's Law states that there is a directed neutron flow (neutron current) from a region of high integral neutron flux to a region of lower integral flux. The mathematical expression for Fick's Law is:

$$\boldsymbol{J}_g = -D_g \boldsymbol{\nabla} \phi_g \tag{1.36}$$

Where $\boldsymbol{J}_g$ is the group neutron current, ϕ_g is group integral neutron flux, and D_g is the group diffusion coefficient. The gradient operator is in the direction of increasing neutron flux. Since the net neutron flow is towards the lower flux, a negative sign precedes the diffusion coefficients. Substituting Eq. (1.36) and integral fluxes into Eq. (1.18) gives the multigroup diffusion equation.

$$-\boldsymbol{\nabla} \cdot [D_g(\boldsymbol{r}) \boldsymbol{\nabla} \psi_g(\boldsymbol{r})] + \Sigma_{a,g}(\boldsymbol{r}) \psi_g(\boldsymbol{r}) + \sum_{g'} \Sigma_{g \to g'}(\boldsymbol{r}) \psi_g(\boldsymbol{r}) = \sum_{g'} \Sigma_{g' \to g}(\boldsymbol{r}) \psi_{g'}(\boldsymbol{r}) +$$

$$\frac{1}{K_{eff}} \sum_{j=i}^{J} \chi_{jg} \sum_g \upsilon \Sigma_{f,j,g}(\boldsymbol{r}) \psi_g(\boldsymbol{r}) \tag{1.37}$$

Where $\Sigma_{g \to g'}(\boldsymbol{r})$ is the macroscopic cross-section for a neutron to scatter out of the energy group g and into group g' and is known as out scattering. $\Sigma_{g' \to g}(\boldsymbol{r})$ is the macroscopic cross-section for a neutron to scatter from group g' into group g and is known as the in scattering cross-section. The integrated neutron flux and cross-sections has been changed to ψ_g representing the diffusion integral flux to avoid confusion for later discussions.

Full reactor core calculations are normally performed with two energy groups. The first group is known as the fast group, and the group includes all energies greater then

0.625 eV, all other neutron energies are in the second group, known as the thermal group. All neutrons born from fission are always in the fast group, and most neutrons that induce fission have energy within the thermal range. For two energy groups, Eq. (1.37), transforms into a system of two equations, one for the fast group, and one for the thermal group, shown in (1.38).

$$-\boldsymbol{\nabla}\cdot[D_1(\boldsymbol{r})\boldsymbol{\nabla}\psi_1(\boldsymbol{r})]+\bar{\Sigma}_{a,1}\psi_1(\boldsymbol{r})+\bar{\Sigma}_{1\to2}\psi_1(\boldsymbol{r})\ =\bar{\Sigma}_{2\to1}\psi_2(\boldsymbol{r})+$$

$$\frac{1}{K_{eff}}\sum_{j=i}^{J}\chi_j\left(\upsilon\bar{\Sigma}_{f,j,1}\psi_1(\boldsymbol{r})+\upsilon\bar{\Sigma}_{f,j,2}\psi_2(\boldsymbol{r})\right)$$

$$-\boldsymbol{\nabla}\cdot[D_2(\boldsymbol{r})\boldsymbol{\nabla}\psi_2(\boldsymbol{r})]+\bar{\Sigma}_{a,2}\psi_2(\boldsymbol{r})+\bar{\Sigma}_{2\to1}\psi_2(\boldsymbol{r})\ =\bar{\Sigma}_{1\to2}\psi_1(\boldsymbol{r}) \qquad (1.38)$$

1.3. Standard Homogenization

Solving the transport equation for a full reactor core or lattice is computationally expensive and not practicable for production calculations given the time and cost constraints. Instead, the transport equation is solved on a small region that is repeated throughout the reactor lattice, known as a cell. The cross-section data and diffusion coefficients are then averaged over the region and condensed into two energy groups and then used to solve the full lattice geometry using the computationally cheap diffusion approach. The procedure just described is referred to as homogenization. For homogenization to be useful certain heterogenous reactor properties must be reproduced when the homogenized problem is solved. The homogenization procedure does not allow for conservation of any parameters that characterize any sub-region of the cell, instead the desired conservation will be with regards to the spatial integral of the parameters of

interest. The most commonly employed homogenization method (Standard Homogenization) only requires the reaction rates to be preserved and utilizes a net zero neutron current ($\boldsymbol{J_g} \cdot \boldsymbol{N} = 0$) on the cell edges during the transportation calculation (Smith, 1984). Standard homogenization is usually performed with use of flux-weighted averages over the entire lattice cell, and the calculation is performed with the following expressions.

$$\bar{\Sigma}_{\alpha g} \int_{V_i} \psi_g(\boldsymbol{r}) d\boldsymbol{r} = \int_{V_i} \phi_g(\boldsymbol{r}) \Sigma_{\alpha g}(\boldsymbol{r}) d\boldsymbol{r} \tag{1.39}$$

$$\bar{\Sigma}_{\alpha g} = \frac{\int_{V_i} \phi_g(\boldsymbol{r}) \Sigma_g^{\alpha}(\boldsymbol{r}) d\boldsymbol{r}}{\int_{V_i} \phi_g(\boldsymbol{r}) d\boldsymbol{r}} \tag{1.40}$$

$$\bar{D}_g = \frac{\int_{V_i} \phi_g(\boldsymbol{r}) D_g(\boldsymbol{r}) d\boldsymbol{r}}{\int_{V_i} \phi_g(\boldsymbol{r}) d\boldsymbol{r}} \tag{1.41}$$

Where V_i, ψ_g, $\bar{\Sigma}_{\alpha g}$, and $\bar{D}_g$ are the volume of the lattice cell, the homogenized integrated flux, the homogenized cross-section, and the homogenized diffusion coefficient respectively. The corresponding heterogenous parameters are denoted by ϕ_g, $\Sigma_{\alpha g}$, and D_g representing the integrated neutron flux, macroscopic cross-section, and the diffusion coefficient respectively. The subscript α denotes the type of cross-section which can be: out scattering, in scattering, absorption, or fission.

The process of homogenization of a PHWR lattice is depicted in Figure 1.2. The two-dimensional lattice cell for PHWRs is normally taken to be the cross-section of a single fuel-bundle and its surrounding tubes (depicted on the left of Figure 1.2 as the circle inside the lattice cell) and moderator (depicted as the light blue surrounding the circles in the left of Figure 1.2). The PHWR lattice cell is shown in more detail in Figure 2.1 and will be further described in Section 2.1.

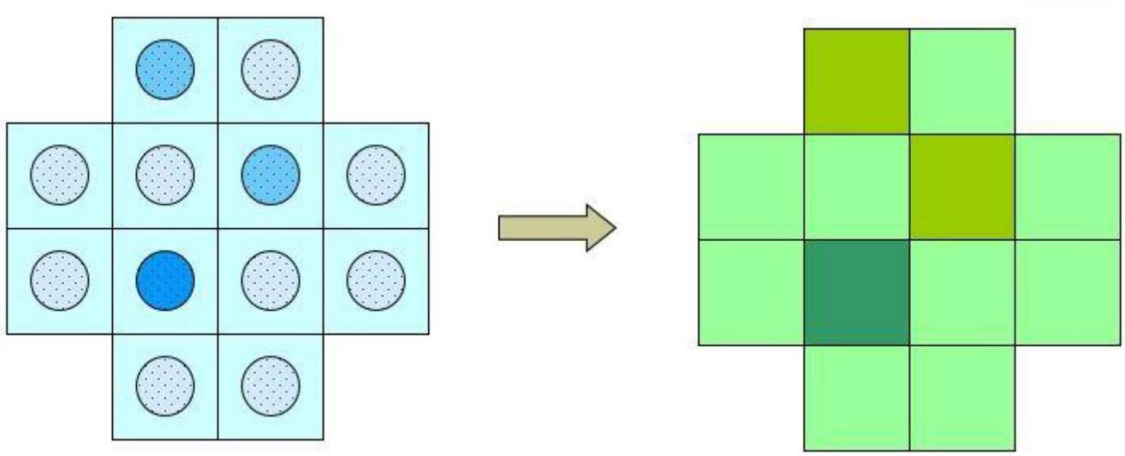

Figure 1.2: Graphical representation of Standard Homogenization for PHWRs (Nichita, 2015).

The difference colours in Figure 1.2 indicate different levels of burnup that come from online refuelling that is done during PHWR operation. Due to the large amount of heterogeneity that is present in a PHWR, error is introduced when homogenization is applied. The focus of this thesis is to improve the accuracy of homogenization for PHWRs, by performing sub-cell homogenization with equivalent factors and accounting for cell-boundary leakage.

Chapter 2: Literature Review and Problem Statement

2.1 Problems with Standard Homogenization

2.1.1. The PHWR Lattice Cell

The standard lattice cell (or node) that is used for PHWR calculations normally represents a single fuel bundle and all the surrounding materials including the heavy water moderator. The lattice cell is square with side lengths of 28.575 cm as shown in Figure 2.1. The fuel bundle is made up of thirty-seven fuel pins, consisting of natural uranium oxide fuel pellets incapsulated in a zircaloy tube. The fuel pins are arranged in a concentric-ring configuration, with a single pin in the centre surrounded by a ring of six pins, a ring of twelve pins, and an outer-most ring of eighteen pins. The fuel bundle is surrounded by heavy water coolant (99.7% pure at ~550K) and contained inside a pressure tube made of Zr-Nb 2.5% alloy. The pressure tube is within a zircaloy calandria tube. To ensure thermal isolation between the hot fuel channel and the cool moderator the calandria tube and pressure tube are separated by an annulus gap filled with helium gas. The calandria tube is surrounded by a large volume of 99.9% pure heavy water moderator at 346K. The high heterogeneity present in the PHWR lattice causes standard homogenization to introduce large homogenization errors.

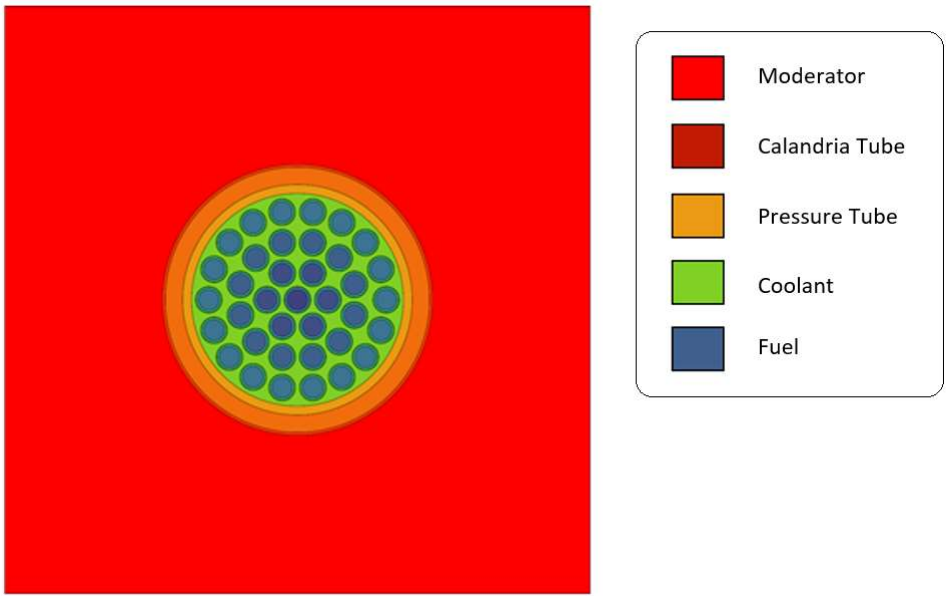

Figure 2.1: Standard PHWR Two-Dimensional Lattice Cell.

2.1.2. Homogenization Errors

The quantities that are required to be preserved for a homogenized model to give equivalent results to a heterogenous model include the multiplication constant, the cell averaged reaction rate (which requires Eq. (1.39) to hold true), and surface averaged current (which requires Eq. (2.1) to hold true).

$$\int_{s_i^k} \nabla \cdot \boldsymbol{J_g}(\boldsymbol{r}) \cdot dS \; = \int_{s_i^k} \nabla \cdot \bar{\boldsymbol{J}}_{\boldsymbol{g}}(\boldsymbol{r}) \cdot dS \tag{2.1}$$

In Eq. (2.1) s_i^k represents face k of region i; $\boldsymbol{J_g}$ is the heterogenous group neutron current and $\bar{\boldsymbol{J}}_{\boldsymbol{g}}$ is the homogenous group neutron current. When using diffusion theory, Eq. (2.1) requires the homogenous diffusion coefficient to be determined from Eq. (2.2).

$$\bar{D}_g^i = \frac{-\int_{s_i^k} \boldsymbol{J_g}(\boldsymbol{r}) \cdot dS}{\int_{s_i^k} \nabla \cdot \psi_g(\boldsymbol{r}) \cdot dS} \tag{2.2}$$

However, it is impossible to have spatially constant values for $\overline{D}_g^i$ that preserve both reaction rates and surface currents. To overcome this problem either additional degrees of freedom are necessary or some of the of preservation requirements need to be relaxed. The standard homogenization procedure relaxes the preservation requirements needed and focuses on the preservation of reaction rates only (Smith, 1986). The generated cross-sections determined from standard homogenization do not conserve the reaction rates from transport to diffusion calculations. The main reason for the inaccuracies come from the net zero cell boundary current assumption and the definition of the homogenized diffusion coefficient presented in Eq. (1.41). The argument for the validation of these assumptions is that for an infinite lattice consisting of identical cells standard homogenization will preserve the reaction rates. However, if there are finite boundaries present on the reactor or cells are not identical (e.g. fuel is at different burnup levels, or a control rod is present) then the reaction rates are not preserved. The disagreement is illustrated by the inaccurate results from standard homogenization when cobalt absorption rods were introduced at the Pickering power plant (Robinson, 1995). Improvement of full reactor core calculations is required and has been an active area of research in recent years.

2.2. Historical Improvements for Homogenization

There has been considerable effort in the past forty years to develop improved homogenization methods. One such method is known as Generalized Equivalence Theory and it allows preservation of reaction rates from the transport model to the diffusion

model (Smith, 1980). The inter-lattice leakage is corrected by enforcing discontinuity of the integral flux at the inter-cell boundaries. The discontinuities are expressed by imposing the continuity of the product between the flux and quantities called discontinuity factors given by the following expression:

$$f_g = \frac{\phi_g^b}{\bar{\psi}_g^b} \tag{2.3}$$

Where ϕ_g^b and $\bar{\psi}_g^b$ are the heterogenous and homogenous integral neutron fluxes at boundary b for group g. Discontinuity factors can be calculated for each cell boundary. The generation of the discontinuity factors require some computational steps in addition to the two steps in the Standard Homogenization approach.

The idea of discontinuity factors was further built upon by use of a linear discontinuous finite difference diffusion formulation which applied discontinuous factors to the diffusion model (Aragones & Anhert, 1986). The method applied limited incremental corrections to the diffusion coefficients and was able to achieve faster and steady convergence of eigenvalues for lattice cells surrounded by high neutronic reflecting boundaries. The main limitation of the method was that it had a requirement of incremental correction calculations done separately between each local and global calculation step. A method that utilized a linear interpolation scheme to correct the homogenized cross-sections and discontinuity factors was investigated (Rahnema & Nichita, 1997). The homogenized parameters computed from the transport equation were subjected to interpolation and then along with the discontinuity factors were independently related to the surface current ratio at each surface. The parameters were corrected based on the actual boundary conditions for each lattice cell boundary. The

method, however, could only successfully be applied to diffusion theory for LWRs due to their cartesian arrangement of the fuel assemblies.

A method that achieved similar results to the discontinuity factors was generating lattice cell cross-sections as a function of the boundary conditions (Rahnema, 1989). The variation of inter-lattice leakage was originally accounted for through use of boundary condition perturbation theory. However, was latter improved upon by Kim and Cho (1993) to avoid the use of perturbation theory by applying an iterative approach for generating lattice cell cross-sections with flux weighted constants and variational principles (Pomraning, 1967). The method was able to reduce the computational cost but was only ever applied to LWRs and Boiling Water Reactors (BWRs). Another alternative to discontinuity factors was investigated that utilized a function fitting method that incorporated the surrounding effects on the generated cross-sections (Herrero et al., 2012). A simplified Analytic Coarse Mesh Finite Difference function that neglected the interacting energy group terms was used for generation of cross-sections. The effects of the interacting energy group terms were instead accounted for in the cell buckling calculations. The result of the method produced good cross-sections for diffusion pin-by-pin calculations. More recently, an alternative approach was put forward by Berman (2013) that introduced weakly space-dependent diffusion coefficients, which allowed for improved preservation of averaged group reaction rates and surface currents. The method made use of an iterative approach, known as the iterative semi-homogenization method. The results were evaluated with a set of one dimensional, one group test problems and compared to other methods. The method was found to be highly successful at preserving reaction rates and surface currents.

Another important alternative approach for improvement of Standard Homogenization process is Superhomogenization or SPH (Herbert, 1993). Superhomogenization has the benefit of being computationally inexpensive in comparison to its contemporaries. The SPH method is the approach used in this study and will be further expanded on in the following section.

2.3. Superhomogenization

2.3.1. History of SPH in Literature

The SPH procedure has been iterated upon over the course of its development history. The method can be broken down into three generations during its development. The first generation was the inception of the approach and was first presented by Kavenoky (1978). The first attempt was to try and create SPH-corrected homogenized cross-sections for a heterogenous diffusion model of an irregular LWR lattice. The procedure renormalized the homogenized cross-sections and fluxes to conserve reaction rates and node boundary currents in a simplified assembly calculation or macrocalculation. The macrocalculation is performed over assembled homogenized pin cells with uniform cell boundary currents in a coarse energy grid. The number of SPH factors that were generated for each coarse energy group is equal to the number of pin cells, and the method was only shown to be consistent when the number of surface currents were equal to the number of SPH factors. As a result, this limited the approach to situations where each pin cell was surrounded by a uniform surface current.

Carrying over some of the ideas from the first generation, Herbert (1981) presented the second-generation procedure for SPH. The second-generation provides a transport-

transport and transport-diffusion equivalence technique that removes the limitations of the first generation by determining a consistent set of SPH factors regardless the number of cell boundary currents. This was achieved by performing a steepest decent search to obtain SPH factors that conserve reaction rates in the macrocalculation. The gradients were determined by use of general perturbation of the macrocalculation. The method generates an infinite number of SPH factor sets and requires normalization to determine a unique SPH factor set. The factors were normalized to conserve the integrated flux of the global assembly.

The third generation was a direct iterative improvement of the second generation with addition of more SPH factor normalization options and a simplified iterative strategy for determining SPH factors that no longer requires using a general perturbation of the macrocalculation.

The third generation SPH method as applied to LWR was presented by Herbert (1993). The results showed promise with the control rod worth measurements of a pin-by-pin sub-cell homogenization with SPH factors in comparison to reference values. Recently an investigation into the SPH method applied to PHWR was performed (Mohapatra, 2016) and will be discussed in detail in the following section.

2.3.2. Theoretical Background

The Superhomogenization (SPH) method, is a sub-cell homogenization approach with equivalent factors or SPH factors used to correct homogenized cross-sections and diffusion coefficients. The SPH factors insure conservation of reaction and leakage rates from fine region and fine group transport model to a coarse region and coarse group

diffusion model. The SPH adjusted cross sections are determined from multiplying the averaged cross section, $\bar{\Sigma}_{m,k}$, for a coarse region $C_m$and group $M_k$by the correlating SPH factor, $\mu_{m,k}$.

$$\widetilde{\mathrm{D}}_{m,k} = \mu_{m,k}\overline{\mathrm{D}}_{m,k}$$

$$\tilde{\Sigma}_{m,k} = \mu_{m,k}\bar{\Sigma}_{m,k} \tag{2.4}$$

The SPH factors ensure the conservation of reaction rates, which can be expressed with average heterogenous flux, $\bar{\phi}_{RG}$, and the averaged diffusion flux, $\bar{\psi}_{RG}$, for coarse region R and group G as the following:

$$\tilde{\Sigma}_{m,k}\bar{\psi}_{m,k} = \bar{\Sigma}_{m,k}\bar{\phi}_{m,k} \tag{2.5}$$

The relationship between the average homogenous flux and heterogenous flux is then:

$$\bar{\phi}_{m,k} = \mu_{m,k}\bar{\psi}_{m,k} \tag{2.6}$$

The SPH corrected cross sections can then be substituted in the multigroup diffusion Eq. (1.37) to give the SPH corrected multigroup diffusion equation shown in Eq. (2.7).

$$-\boldsymbol{\nabla}\cdot[\widetilde{D}_k(\boldsymbol{r})\boldsymbol{\nabla}\tilde{\psi}_k(\boldsymbol{r})] + \tilde{\Sigma}_{a,k}(\boldsymbol{r})\tilde{\psi}_k(\boldsymbol{r}) + \textstyle\sum_{k'}\tilde{\Sigma}_{k\to k'}(\boldsymbol{r})\tilde{\psi}_k(\boldsymbol{r}) = \sum_{k'}\tilde{\Sigma}_{k'\to k}(\boldsymbol{r})\tilde{\psi}_{k'}(\boldsymbol{r}) +$$

$$\frac{1}{K_{eff}}\textstyle\sum_{j=i}^{J}\chi_{jk}\sum_k \nu\tilde{\Sigma}_{f,j,k}(\boldsymbol{r})\tilde{\psi}_k(\boldsymbol{r}) \tag{2.7}$$

The two-group diffusion system of equations can also be written in terms of SPH corrected cross-sections and diffusion coefficients buy substituting them into Eq. (1.38) to get Eq. (2.8).

$$-\boldsymbol{\nabla}\cdot[\widetilde{D}_1(\boldsymbol{r})\boldsymbol{\nabla}\tilde{\psi}_1(\boldsymbol{r})] + \tilde{\Sigma}_{a,1}(\boldsymbol{r})\tilde{\psi}_1(\boldsymbol{r}) + \tilde{\Sigma}_{1\to 2(r)}\tilde{\psi}_1(\boldsymbol{r}) = \tilde{\Sigma}_{2\to 1}(\boldsymbol{r})\tilde{\psi}_2(\boldsymbol{r}) +$$

$$\frac{1}{K_{eff}}\sum_{j=i}^{J}\chi_j\left(\nu\tilde{\Sigma}_{f,j,1}(\boldsymbol{r})\tilde{\psi}_1(\boldsymbol{r})+\upsilon\tilde{\Sigma}_{f,j,2}(\boldsymbol{r})\tilde{\psi}_2(\boldsymbol{r})\right)$$

$$-\boldsymbol{\nabla}\cdot[\tilde{D}_2(\boldsymbol{r})\boldsymbol{\nabla}\tilde{\psi}_2(\boldsymbol{r})]+\tilde{\Sigma}_{a,2}(\boldsymbol{r})\tilde{\psi}_2(\boldsymbol{r})+\tilde{\Sigma}_{2\to1}(\boldsymbol{r})\tilde{\psi}_2(\boldsymbol{r})\ =\tilde{\Sigma}_{1\to2}(\boldsymbol{r})\tilde{\psi}_1(\boldsymbol{r}) \quad (2.8)$$

The neutron fluxes determined from Eq. (2.8) should give the same value as the neutron flux determined from Eq. (1.18) for the same reactor geometry and material composition after normalization.

The SPH factors are calculated by an iterative method. The approach that was chosen is a fixed-point iterative strategy and allows avoidance of general perturbation of the macrocalculation. The algorithm proceeds in four steps:

1. The SPH factors are set to unity for iteration 0

$$\mu_{m,k}^{(0)}=1 \quad (2.9)$$

The neutron source is then estimated by:

$$Q_k^{(0)}(\boldsymbol{r})=\sum_l Q_{m,k\leftarrow l}\ \ if\ \boldsymbol{r}\in V_m \quad (2.10)$$

2. The SPH factors are used to generate the corrected cross and diffusion coefficients with Eq. (2.4). A macrocalculation can then be performed with conservative boundary conditions to obtain the macro flux $\tilde{\psi}_k^{(n)}(\boldsymbol{r})$, for each coarse energy group as a function of the neutron sources of the preceding iteration. The macro integrated flux can then be determined by:

$$\tilde{F}_{m,k}^{(n)}=\int_{V_m}d^3r\tilde{\psi}_k^{(n)}(\boldsymbol{r}) \quad (2.11)$$

3. The macro integrated flux can then be used to determine the SPH factors by Eq. (2.12), where $F^*_{m,k}$ is the target integrated reaction rate and is given by Eq. (2.13).

$$\mu^{(n)}_{m,k} = \frac{F^*_{m,k}}{\tilde{F}^{(n)}_{m,k}} \tag{2.12}$$

$$F^*_{m,k} = \sum_{g\in M_k}\sum_{i\in C_m} V_i \phi_{i,g} \tag{2.13}$$

4. If the following convergence criterion is satisfied by the current iteration of the SPH factors, then the procedure is complete.

$$\max_{m,k} \frac{\left|\mu^{(n)}_{m,k} - \mu^{(n-1)}_{m,k}\right|}{\mu^{(n)}_{m,k}} < 10^{-4} \tag{2.14}$$

If the criterion is not satisfied, n is set to $n+1$ and the iteration is repeated starting at step 2.

There are an infinite number of SPH factors that can satisfy the conservation of the macrocalculation for a closed geometry (reflective boundary conditions) that differ up to a single multiplication constant that is the same for all regions and groups. To obtain a unique solution, the SPH factors are determined with an arbitrary normalization condition. The most common and simplest condition is the flux-volume normalization condition. The normalization is done by normalizing the flux determined in step two of the iteration process (Herbert, 2009).

$$\tilde{\psi}^{(n)\ norm.}_k(\boldsymbol{r}) = \tilde{\psi}^{(n)}_k(\boldsymbol{r}) \frac{\sum_m F^*_{m,k}}{\sum_m \int_{V_m} d^3 r \tilde{\psi}^{(n)}_k(\boldsymbol{r})} \tag{2.15}$$

Similarly, to the case of standard homogenization SPH full reactor core calculation proceeds in two steps. The first step differs however, in the fact that homogenization is

done at a sub-cell level and SPH equivalence factors are determined in an iterative method. Once the sub-cell homogenized and group condensed cross-sections are determined and SPH corrected, the full core diffusion model is constructed, and neutron fluxes are calculated. Due to the Cartesian geometry of LWRs, SPH can be done on a pin-by-pin level, a graphical representation of the Superhomogenization full core calculation for LWR is shown in Figure 2.2. The heterogenous pin sub-region of the fuel assembly is shown on the left of Figure 2.2. The sub-region is homogenized, and the resulting cross-sections are corrected with SPH factors, as illustrated by the centre image in Figure 2.2. The SPH corrected homogenized sub-region is then used to construct the full reactor core depicted on the right of Figure 2.2.

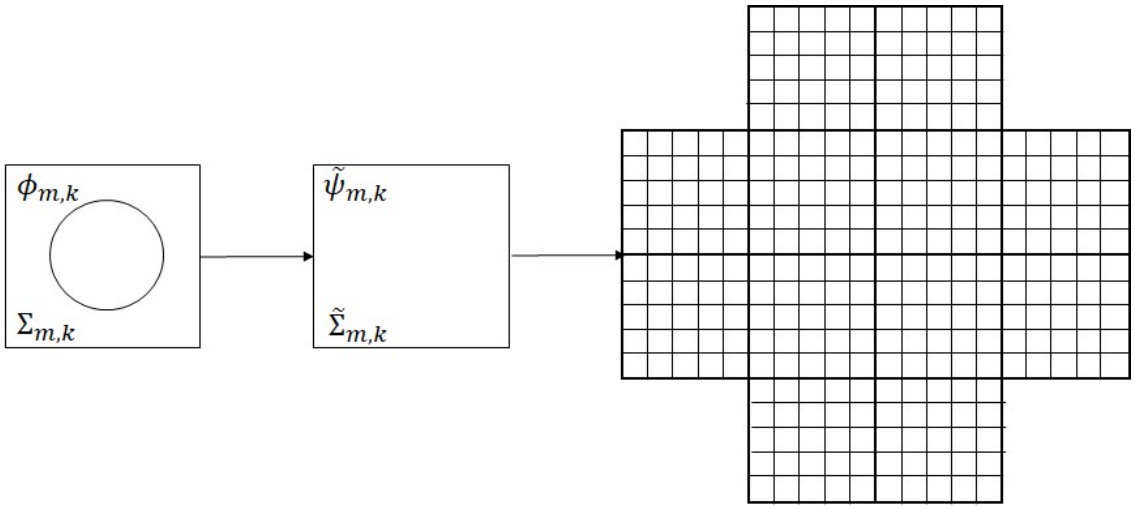

Figure 2.2: Sub-cell SPH homogenization for LWRs.

2.4. Thesis Problem Statement

There is considerable interest in utilizing the SPH method for production of PHWRs since it circumvents additional computational steps that are required for other homogenization improvement methods. More importantly, it can easily be implemented into current production algorithms since no change to the current computational infrastructure is required, only changing the cross-section and diffusion coefficients that are used. The SPH method has had limited investigation in the past into its application to diffusion models with PHWR geometries but has shown promise in its application to LWRs. Recently, a sub-cell homogenization diffusion model using SPH equivalence factors has been applied to PHWRs, however the results did not show significant or any improvement of the standard homogenization approach (Mohapatra, 2016). The investigation performed sub-cell homogenization on a single PHWR lattice cell with reflective boundary conditions. The SPH factors were normalized using the flux-volume normalization condition. The SPH corrected cross-sections were then utilized in a 3×3 lattice cell partial core macrocalculation with discharge burnup bundles present for assessment of the method. The results were compared to a reference equivalent heterogenous transport partial core model. There was no improvement of the method when results were compared with an equivalent standard homogenization approach. Table 2.1 shows the comparison of SPH factors for all nine sub-regions of the lattice cell calculated from a single lattice cell calculation and from a 3×3 lattice cell calculation. The single cell SPH factors are shown on the top row for each of the nine sub-regions. The percent difference of the single cell SPH factors compared to the exact SPH factors for the top left lattice cell from the 3×3 calculation is shown in the middle row for each

sub-region. The percent difference of the single cell SPH factors compared to the exact SPH factors for the centre lattice cell from the 3×3 calculation is shown in the bottom row for each sub-region. Table 2.1 shows a several percent difference between the single cell SPH factors and the exact SPH factors generated using a 3×3 partial core model. The difference suggests that the SPH factors are dependent on cell-boundary leakage, and further investigation for possible improvement with a better description of cell boundary conditions was recommended.

Table 2.1: SPH factor comparison (Nichita & Mohapatra, 2016).

SPH facts. (single-bundle)	1.009	1.042	1.009
% diff. (top left)	11.79	11.31	10.39
% diff. (centre)	6.26	4.05	1.41
SPH facts. (single-bundle)	1.042	0.889	1.042
% diff. (top left)	11.31	10.85	9.86
% diff. (centre)	4.05	1.38	-1.65
SPH facts. (single-bundle)	1.009	1.042	1.009
% diff. (top left)	10.39	9.86	8.62
% diff. (centre)	1.41	-1.65	-4.55

The work presented herein will directly build upon the method used in the previous attempt to apply SPH to PHWRs with improved cell-boundary leakage descriptions.

Chapter 3: Methodology

The following presents the methodology utilized in this research for generating SPH factors and evaluating the SPH method with corrected boundary conditions as applied to PHWRs. As mentioned previously, sub-cell SPH corrected homogenization reactor calculations proceed in two steps; a lattice calculation and a core calculation. The first step, the lattice calculation, is a transport calculation done, typically on a single cell with detailed geometry and 69 energy groups and includes energy condensation and coarse sub-cell geometry homogenization. During this step, SPH factors are calculated along with the sub-cell homogenized cross-sections and diffusion coefficients. To ensure accurate boundary conditions, the lattice calculation step was performed for a multi-cell model (usually a 3×3-cell model consisting of the cell of interest surrounded by its 8 neighbors) and not for an isolated lattice cell with reflective boundary conditions. Including the surrounding cells in the model ensures that the boundary conditions for the cell of interest (located at the center of the super-cell) are close to the true ones present in a full-core calculation. Aside from the usual 3×3 super-cell, additional super-cell models were used to account for corner, centre, and side lattice cell positions in the full-core geometry. The different multi-cell geometries used are shown in Figure 3.1 below.

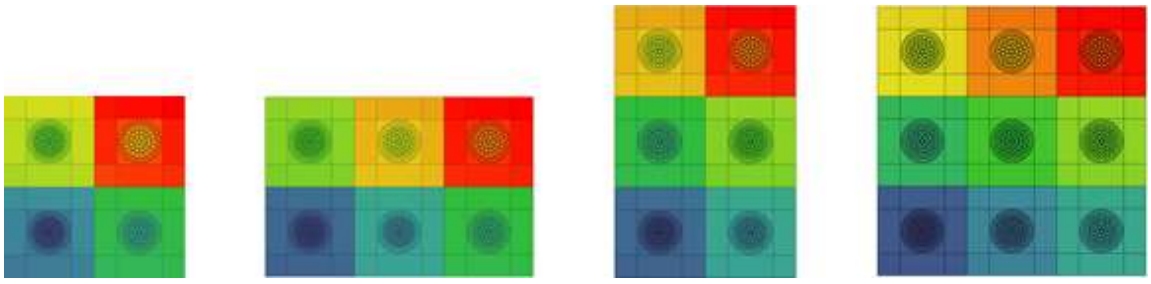

Figure 3.1: The different multi-cells used for the lattice calculations.

The centre cell's (or corner or side lattice cell) SPH factors, homogenized cross-sections and diffusion coefficients were the ones used for the core calculation step. The full-core model employed in this work was a 5×5-cell core, which was small-enough to allow a reference flux to be found using transport theory for the detailed, heterogeneous, geometry. The full core calculation was also referred to as a homogeneous diffusion calculation. The homogenized core model was constructed by assembling together the sub-cell homogenized cells and is shown in Figure 3.2.

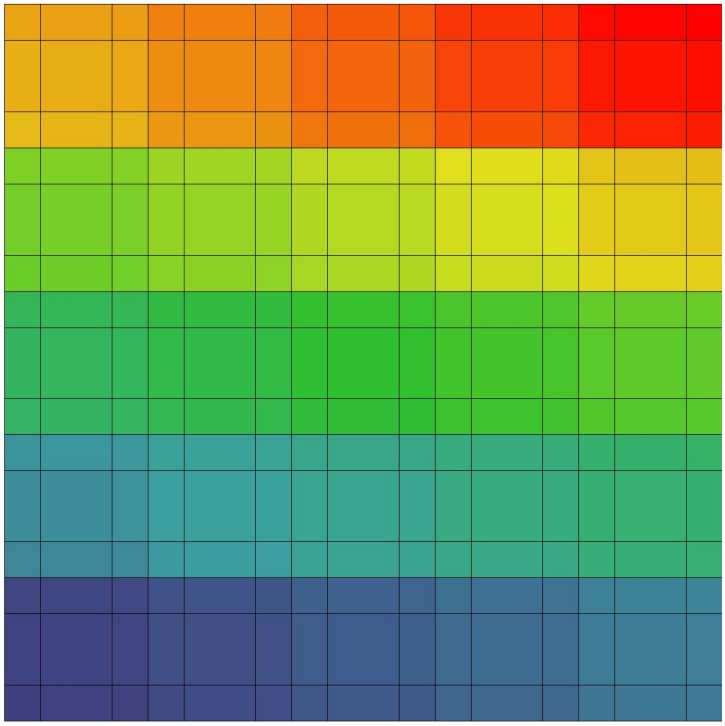

Figure 3.2: Sub-cell homogenized 5×5 reactor core.

The macroscopic cross sections for the homogenized cells were determined from the (multi-cell) lattice calculation for each respective lattice cell location in the reactor core. For lattice cells in the corner of the 5×5 core, the SPH factors and cross-sections were taken from a 2×2 multi-cell calculation with an equivalent burnup pattern. For lattice

cells on the edge of the core data from one of the two centre cells from the 3×2 multi-cell calculations with an equivalent burnup pattern were used, the specific cell was dependent on the orientation within the core. For lattice cells inside the core the data from the centre cell of the 3×3 multi-cell with an equivalent burnup pattern was used. An illustration demonstrating the origin of the data used in each lattice cell is depicted in the Figure 3.3 below.

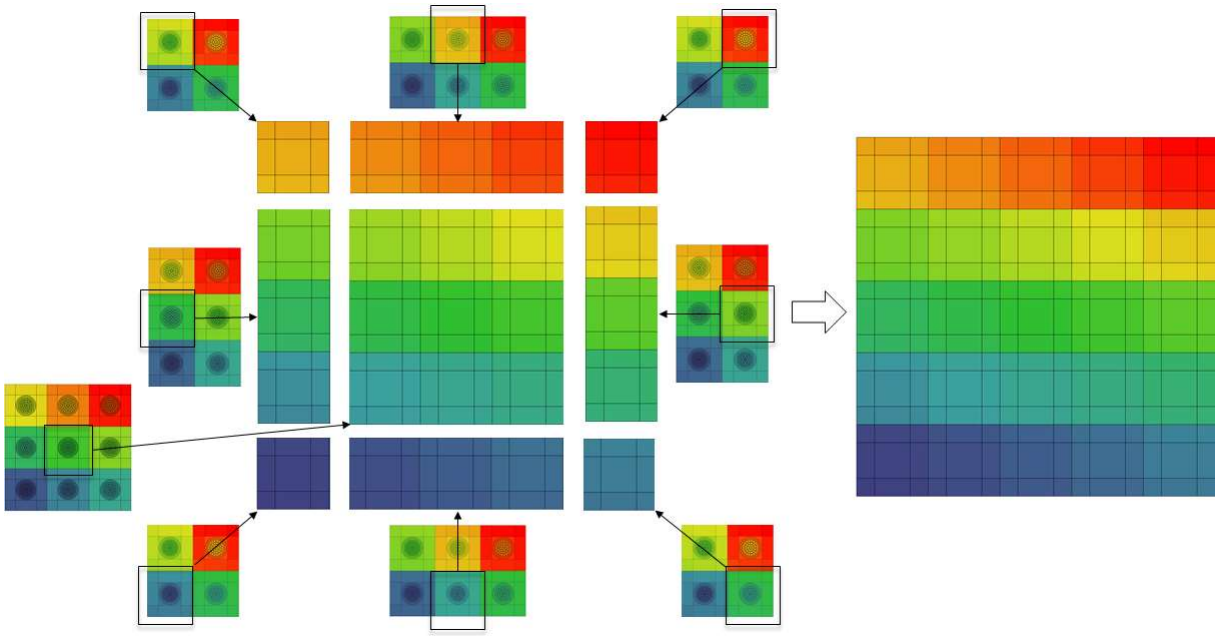

Figure 3.3: Illustration of the construction of the diffusion core from the data of the super-cell calculations.

The neutron fluxes and reaction rates were then compared to the reference ones obtained from the detailed-geometry full-core transport calculation.

3.1. Fuel Burnup considerations

Unique to PHWRs is online refueling, which creates an additional consideration for analysis of PHWRs. Due to online refueling, different lattice cells can have different

levels of fuel burnup. Such differences need to be accounted for when modelling the reactor core because macroscopic cross-sections change with the fuel burnup. The burnup of a single PHWR lattice cell was simulated using 69-energy groups using the microscopic cross-section library developed by the WIMS-D Library Update Project (WLUP) (Jonkmans, 2006). The boundary conditions were reflective, however, during production the reactor runs at criticality so a B_1 type calculation was performed. A B_1 type calculation enforces a k_{eff} of 1 and introduces buckling as the eigenvalue for the transport equation and effectively adjust the lattice cell leakage to maintain a critical lattice cell. The final results of this calculation consisted of detailed geometry cross-section data condensed to two energy groups. Such cross-sections were generated for multiple burnup levels of the fuel bundle, starting at zero burnup (fresh fuel) to discharge burnup (~7.0 kWd/kg). This new generated cross-section library was used for the following calculations.

3.2. Lattice Calculations

The PHWR lattice cell, as shown in Figure 2.1, was subdivided into 9 rectangular sub-regions, the outer eight consists of just moderator while the ninth, centre sub region contains the entire fuel bundle, pressure tube, calandria tube, and some surrounding moderator, the subdivisions of the lattice cell are shown in Figure 3.4 below.

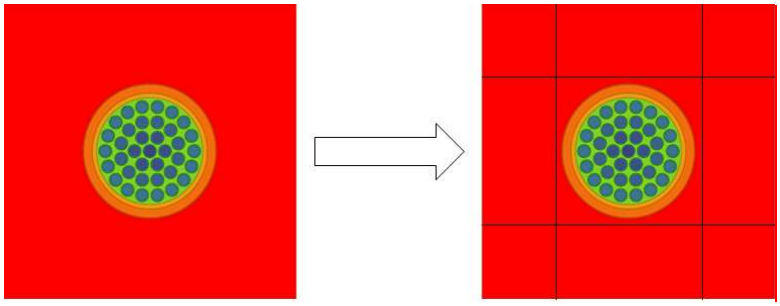

Figure 3.4: Subdivisions of the lattice cell.

Because SPH-corrected cross-sections were used in core diffusion calculations that use Cartesian meshes, the sub-cells for which SPH factors are calculated must be rectangular. At the same time, the PHWR fuel bundle has cylindrical geometry, which does not lend itself to meaningful rectangular sub-divisions and limits the amount of subdivisions possible within the fuel bundle because it requires the full fuel channel to be located in a single sub-region.

Four multi-cell models were constructed using subdivided lattice cells: a 3×3, a vertical and a horizontal 3×2, and a 2×2. SPH factors and sub-cell homogenized cross-sections and diffusion coefficients were determined for all four models. To account for the variable burnup across the lattice cells different combination of fresh fuel and discharge fuel lattice cells were considered for all four super-cell types. Specifically, each cell in a multi-cell model has the same burnup as the corresponding cell in the full-core heterogeneous model.

Reflective boundary conditions were applied to the outer boundary of each multi-cell model, and all multi-cell calculations performed were B_1 type calculations.

3.4. Core Calculation

A 5×5 partial core was utilized to simulate the full reactor core. The core calculation was a diffusion calculation performed on a 5×5 cell-homogenized core. The desired fuel bundle burnup composition to be investigated and cell position in the 5×5 core model determined which data to be used from the lattice calculation. The boundary conditions for the core calculation were reflective and the diffusion calculation produced the integrated flux of the reactor.

To determine how well results obtained from the homogenized core diffusion model reproduce the results obtained using the heterogenous model, a reference calculation was required. The reference calculation was a *k* type two-group transport calculation for a 5×5 partial core with detailed geometry. Reflective boundary conditions were utilized on all boundaries. The results were averaged to give single values for integrated flux per energy group for each lattice cell. Because both the static transport and diffusion equations for multiplying media (i.e. media including fissile materials) are homogeneous eigenvalue-eigenvector problems, the flux is only determined up to a multiplicative constant, which was determined by normalizing all fluxes to correspond to one fission per second per lattice cell.

Before proceeding with lattice cell calculations, the computational method had to be verified to ensure it was performing as intended, which was done by an equivalence test. If the lattice calculation is correct, a 5×5 heterogenous calculation with SPH factors generated from an identical 5×5 detailed transport calculation will give the exact same integrated averaged flux as the equivalent 5×5 transport model after normalization.

Figure 3.5 shows a flow chart that gives a summary of the approach for generating a sub-cell homogenized reactor core that was utilized in this thesis.

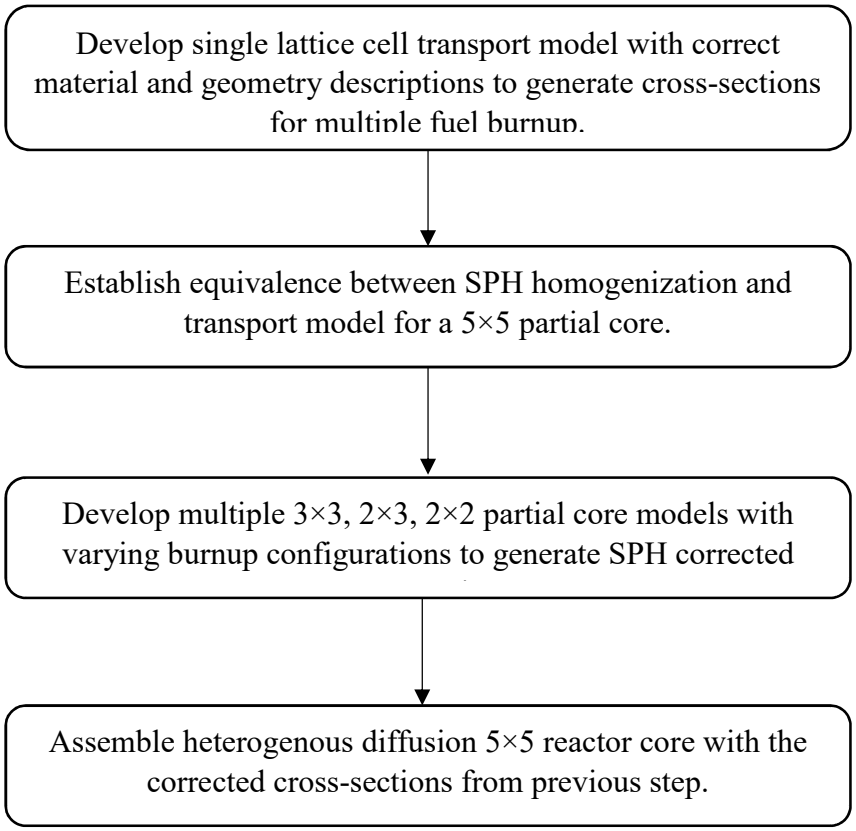

Figure 3.5: Flow chart depicting the methodology used in this thesis.

3.5. Computational Tools

The computational aspect of the research presented here was performed with two standard codes DRAGON and DONJON. For all transport considerations, DRAGON version 3.05E code was utilized and all diffusion considerations were performed with

DONJON version 3.01 code. Both codes were developed at the Ecole Polytechnique de Montreal and are routinely used in the Canadian nuclear industry for lattice and full-core calculations, respectively. This section will present a short description of the two codes.

3.5.1. DRAGON

The computer code DRAGON (Marleau et al., 2007) is a collection of multiple modules that can solve the multi-group neutron-transport equation in complex geometries, specifically in a lattice cell or fuel assembly. It can also perform resonance self-shielding calculations to determine the multigroup cross-sections. Additionally, it can perform fuel depletion calculations and can generate region-homogenized and group-condensed macroscopic cross sections, as well as SPH factors. The various modules are linked together by using the GAN generalized driver and only exchange information between each other by well defined data structures.

The multigroup spatial and angular distribution of the flux as the solution to the neutron transport equation can be determined by various algorithms contained in DRAGON. All algorithms are based on a one-group solution procedure and the contributions from other energy groups are incorporated in the source term. The flux solver algorithms or modules, either utilize collision probability method or the method of characteristics for solving the transport equation. There are five such modules, the first is the JPM option, that solves the integral form of the transport equation using the interface current method applied to homogenous blocks. The following two options are SYBIL and EXCELL/NXT, which solve the integral transport equation using the collision probabilities method, where the former is for simple one-dimensional (1-D) or two-dimensional (2-D) geometries and the latter is for more general 2-D and three-

dimensional (3-D) geometries. The final two modules are MOCC and MCU which both use the method of characteristics to solve the transport equation. For 2-D geometries MOCC is used and for 3-D geometries the MCU module is used. The research presented in this thesis utilized the collision probability method for solving the transport equation for the 2-D PHWR lattice cell and made use of the NXT module.

The DRAGON code requires an input data structure for execution. The data structure is presented as a script using the language CLE-2000, and requires module and variable declaration, geometric description, and nuclear data of the materials simulated within the desired geometry. DRAGON can access microscopic cross-sections directly for desired nuclear data. The geometric parameters and mixture composition as described for a PHWR lattice cell above, along with the WIMS-D WLUP microscopic library were used in this thesis.

3.5.2. DRAGON Modules

Several modules in DRAGON are required for solving the transport equation and generating SPH equivalent factors. These modules include the following: LIB, GEO, NXT, SHI, ASM, FLU, EDI, EVO, and CPO. The LIB module allows the inclusion of the microscopic cross-section library to the definition of the material mixtures. The GEO module allows for the input of the desired geometric description used for the calculation. The NXT module generates the tracking file that allows for general 2-D geometry collision probability method solutions as described above. The SHI module allows for self-shielding calculations at the fuel pin boundary. The ASM module generates the collision probability matrix for the defined geometry. The FLU module generates the flux solution and associated eigenvalues. The EDI module allows for averaging and

condensing cross-sections and generating SPH factors. The information is also stored on a file if needed for later use. The EVO module is used for burnup calculations. The CPO module reorganizes the EDI data structure to a format accessible by DONJON.

3.5.3. DONJON

DONJON computer code (Varin et al., 2005) is used for solving the diffusion equation and nuclear reactor modelling. The code came from merging the diffusion solver code TRIVAC-3 and the reactor modelling code XSIMUL. DONJON is similar to DRAGON in regard to being divided into multiple calculation modules that are all linked together by the GAN generalized driver with exchanging information through well defined data structures. DONJON utilizes multiple spatial discretization in full multigroup formalism to solve the diffusion equation. Due to the application of sub-cell homogenization performed in this research the mesh centred finite differences method is utilized to solve the diffusion equation.

Like DRAGON, DONJON requires a CLE-2000 input data structure for execution of the desired simulated reactor. The input file is required to contain module and variable declaration, the reactor geometric description, and macroscopic cross-section data. The geometry information primarily defines the lattice cells and reflector arrangements. In this study, the geometry portrays the homogenized volume PHWR lattice cells. The macroscopic cross-section data comes from a lattice transport calculation and must be contained in a file with COMPO structure. The DRAGON module CPO produces a COMPO files for a desired lattice calculation to be used in DONJON.

3.5.4. DONJON Modules

The DONJON calculation modules required in the research presented here include the following: GEOM, CRE, BIVACT, BIVACA, FLUD, and OUT. The GEOM module allows for the input of the desired geometric description. The CRE module allows for inclusion of macroscopic cross-section library to the desired material mixtures read directly from a COMPO file. The BIVACT and BIVACA modules are used for generation of tracking information generation depending on the desired calculation method specified to solve the diffusion equation for a two-dimensional geometry. The FLUD module solve the diffusion equation to generate values for the homogenized integrated flux and associated eigenvalues. The OUT module allows for the generation of output files of the computational results.

Chapter 4: Models and Calculations

In this chapter the simulated models used for the lattice calculation step, core calculation step, and the reference partial core calculation are presented. The lattice-cell models that are presented include the single lattice cell for burnup cross-section generation, and the multi-cell models for generating SPH corrected sub-cell homogenized cross-sections. The multiple-burnup core configurations reference models are presented, along with the corresponding heterogeneous diffusion multi-cell models.

4.1. Lattice Calculation models

In this section, the development of the single 69-group detailed transport lattice cell model for DRAGON is presented, along with self-shielding and burnup calculations performed. The calculation produced two-group macroscopic cross-section data for a geometrically detailed lattice cell at multiple fuel burnup levels, from fresh fuel to discharge burnup. The 69 energy groups were condensed to a fast and thermal group, separated at 0.625 eV. The cross-section data from this calculation was then used for all subsequent DRAGON calculations. The multi-cell models used for generating SPH corrected sub-cell homogenized cross-sections are also presented. This section concludes with the diffusion lattice cell model developed for DONJON calculations.

4.1.1. Single-Cell Transport Model

The DRAGON single lattice cell calculation takes the subdivided lattice cell geometric description as discussed in Section 3.3 and material description, along with a microscopic-cross-section library as inputs. The calculation generated an output file that

contains two-group macroscopic cross-sections for multiple levels of fuel burnup in two energy groups. The material composition of the lattice cell was described in Section 2.1.1, and were modelled with the density, isotopic composition (weight %), and temperature presented in Table 4.1 below.

Table 4.1: Material properties within the PHWR lattice cell.

Component	Material	Density (g/cm^3)	Isotopic Composition (weight %)	Temperature (K)
Moderator	D_2O	See below	99.9	346
Calandria Tube	Zircaloy	6.5	100	346
Annulus gap	He	0.0014	100	346
Pressure Tube	Zr-Nb(2.5%) alloy	6.5	100	550
Coolant	D_2O	See below	99.7	550
Fuel Pin	Zircaloy	6.5	100	550
Fuel	UO_2	10.6	See below	1155

The density of heavy water for both the moderator and coolant and isotopic contents of the UO_2 fuel were calculated using the INFO module in DRAGON.

Further spatial discretization of geometric regions improves the computational accuracy in DRAGON at the expense of computational time. The moderator region was further divided to give a 4×4 square, which was sufficient due to the small spatial variation of the neutron flux within the moderator. The fuel channel, however, was subjected to much finer region subdivision. The coolant required annuli subdivisions with thickness between 0.25 to 0.5 the length of the mean free path of a neutron. For heavy water, the mean free path is ~2 cm, which resulted in the thickness of the subdivision in the range of 0.5 to 1 cm (Auger et al., 1947). The fuel pins required further subdivision to account for self-shielding. The resulting DRAGON lattice cell was divided into a total of 179 regions, of

which only 16 were rectangular and the remaining 163 were circular, as depicted in Figure 4.1.

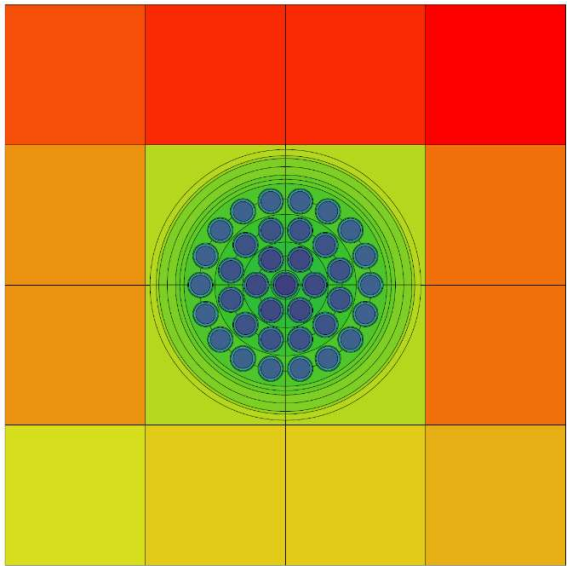

Figure 4.1: Lattice cell generated by DRAGON 3.05E, the different colours represent different mixtures.

After neutron slowing-down occurs in the moderator, neutrons re-entering the fuel pin are susceptible to resonance capture in the fuel. The neutrons that are absorbed are lost on the periphery of the fuel, thus the outer regions shield the centre of the fuel pin creating the effect known as self-shielding. A self-shielding model was used to account for this effect in a lattice cell calculation. The model was an algorithm that produced average (self-shielded) cross-sections defined over a coarse energy group. To achieve the desired cross-sections, sub-regions were assigned to the resonant part of the geometry which subdivide the fuel pin into annuli as depicted in Figure 4.1. The self-shielding calculation was performed by the SHI module in DRAGON.

The final additional consideration required for the single cell lattice calculation is fuel burnup simulation. The burnup calculation was performed by the EVO module in DRAGON. The fuel composition was calculated for fresh fuel and at 7 additional burnup steps, to a maximum burnup of 7000 MWd/t(U). For each burnup step the lattice cell burnup was increased by 1000 MWd/t(U) so by the seventh iteration discharge burnup was achieved. Although there is a rapid change in reactivity from the buildup of fission products and then from the increase in the plutonium concentration, the coarse burnup steps are sufficient since only fresh fuel and discharge burnup fuel was modeled in this thesis.

The data flow during the lattice calculation for a single cell is depicted in Figure 4.2. The final output file was used for subsequent transport calculations.

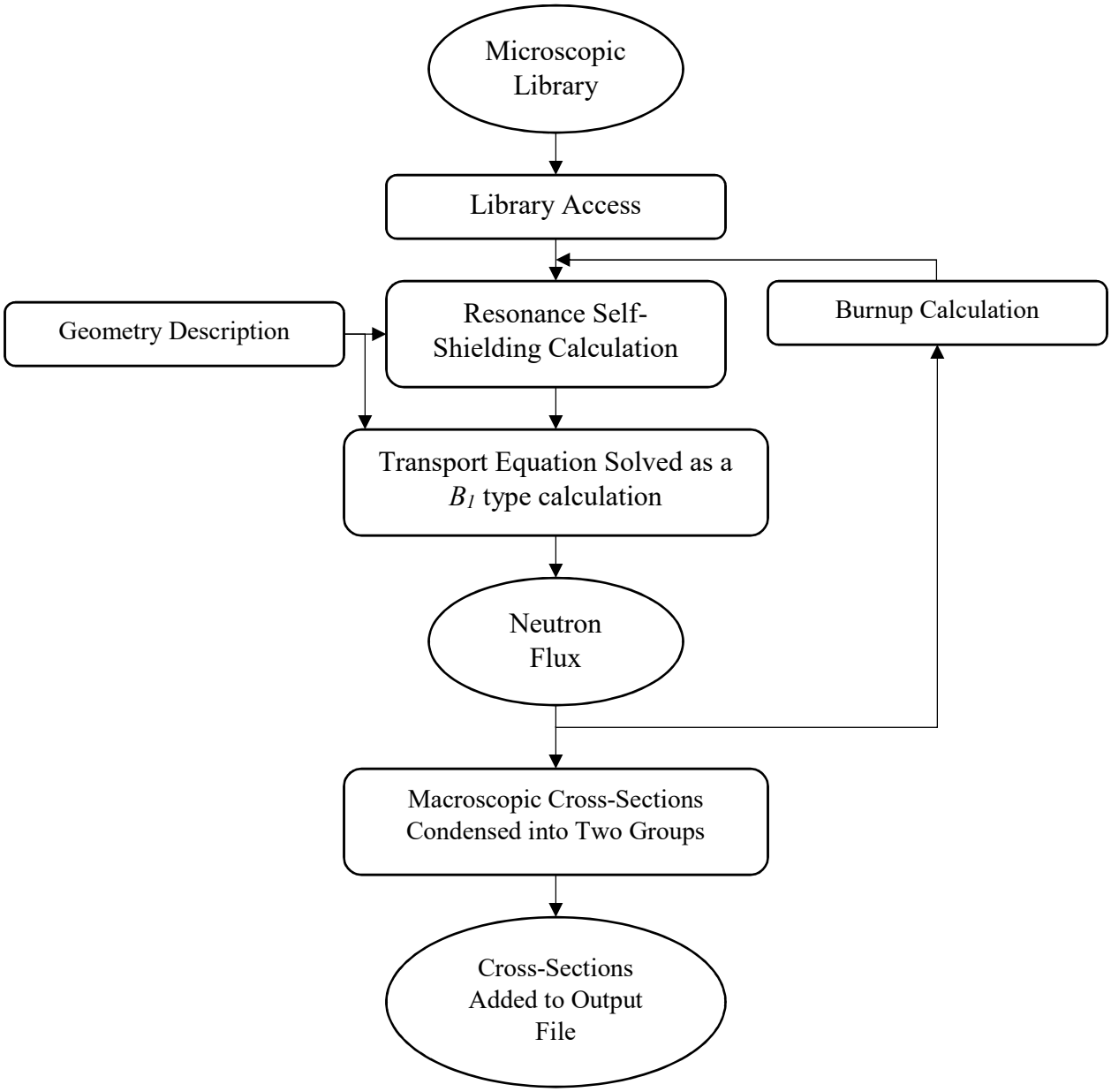

Figure 4.2: Diagram of Data Flow in DRAGON for Single Cell Lattice Calculation.

4.1.2. Multi-Cell Transport Models

A subsequent lattice cell calculation was performed to generate sub-cell homogenized cross-sections with SPH equivalence factors. However, as discussed previously to improve the results with a better description of inter-cell neutron leakage, the calculation was performed using multi-cell models. The multi-cell model was constructed with nine lattice cells as described in Section 4.1.1 to create a 3×3 square model. The boundary conditions were reflective and a B_1 type calculation was performed to simulate a critical reactor. The nine-cell multi-cell model is shown in Figure 4.3.

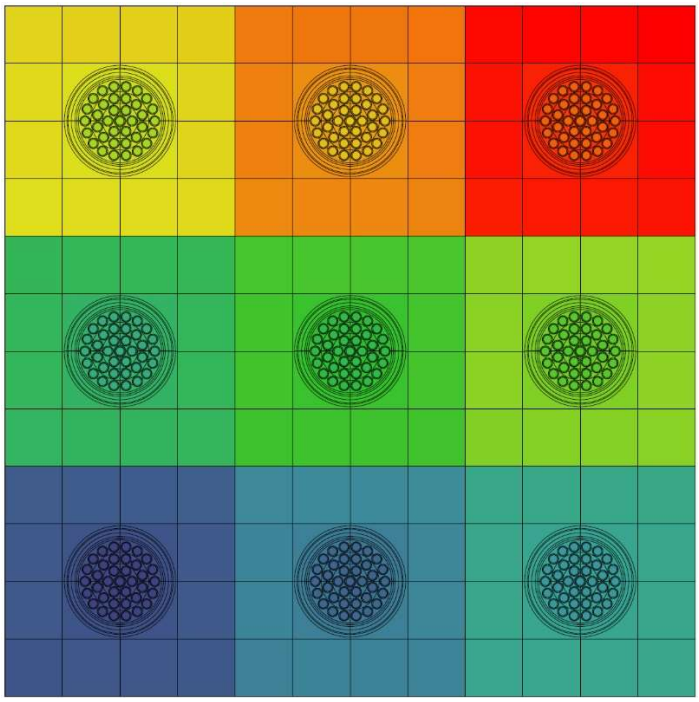

Figure 4.3: 3×3 multi-cell DRAGON 3.05E model for SPH lattice calculations.

The centre cell homogenized cross-sections and SPH factors were transferred to DONJON for core calculations. However, cells located on the corner and edge of the larger core calculation model would not be accurately simulated using the centre 3×3 cell.

Three additional multi-cell calculations were performed for the corner, and edge cells. The corner cell homogenized cross-sections and SPH factors were generated from a 2×2 multi-cell lattice calculation with the same consideration as for the 3×3 model. The data that was transferred to DONJON for subsequent core calculations was taken from the correlating corner of the 2×2 model. The process was repeated but for a six-cell 2×3 model for the edge cells, which required two models to be created: a horizontal and vertical one. The data was generated for one of the middle cells, depending on the location in the core calculation. The three additional models are shown in Figures 4.4 and 4.5 below.

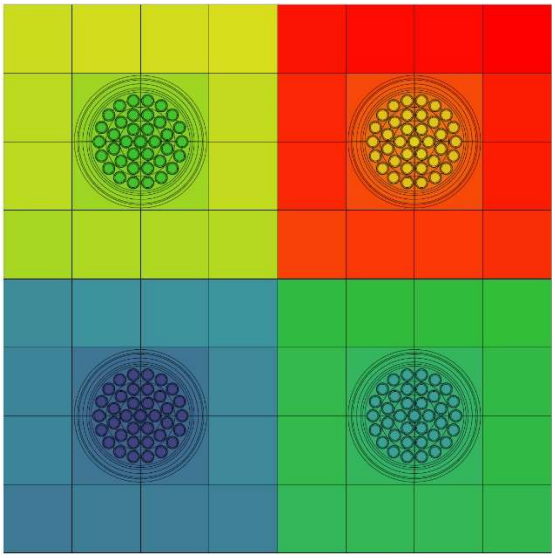

Figure 4.4: 2×2 multi-cell DRAGON 3.05E model for SPH lattice calculation for corner cell in the diffusion core calculation.

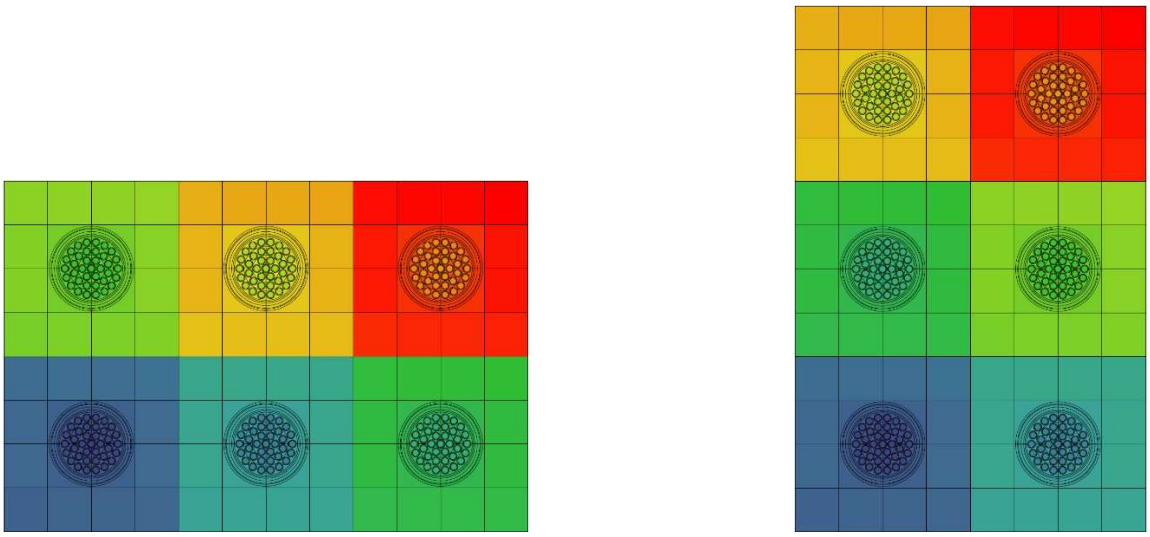

Figure 4.5: Six cell multi-cell DRAGON 3.05E models, both horizontal (left) and vertical (right) for SPH lattice calculation for edge cells in the diffusion core calculation.

The process above was repeated multiple times for varying combinations of fresh fuel bundles and discharge-burnup fuel bundles to allow for several core configurations to be evaluated. The above procedure also allowed generation of full-cell (standard) homogenization without SPH factors for further comparison. Figure 4.6 above shows the data flow within DRAGON for the generation of homogenized cross-sections and SPH factors. The single lattice cell calculation presented in Section 4.1.1 also produced sub-cell homogenized cross-sections with SPH factors, and standard homogenized cross-sections.

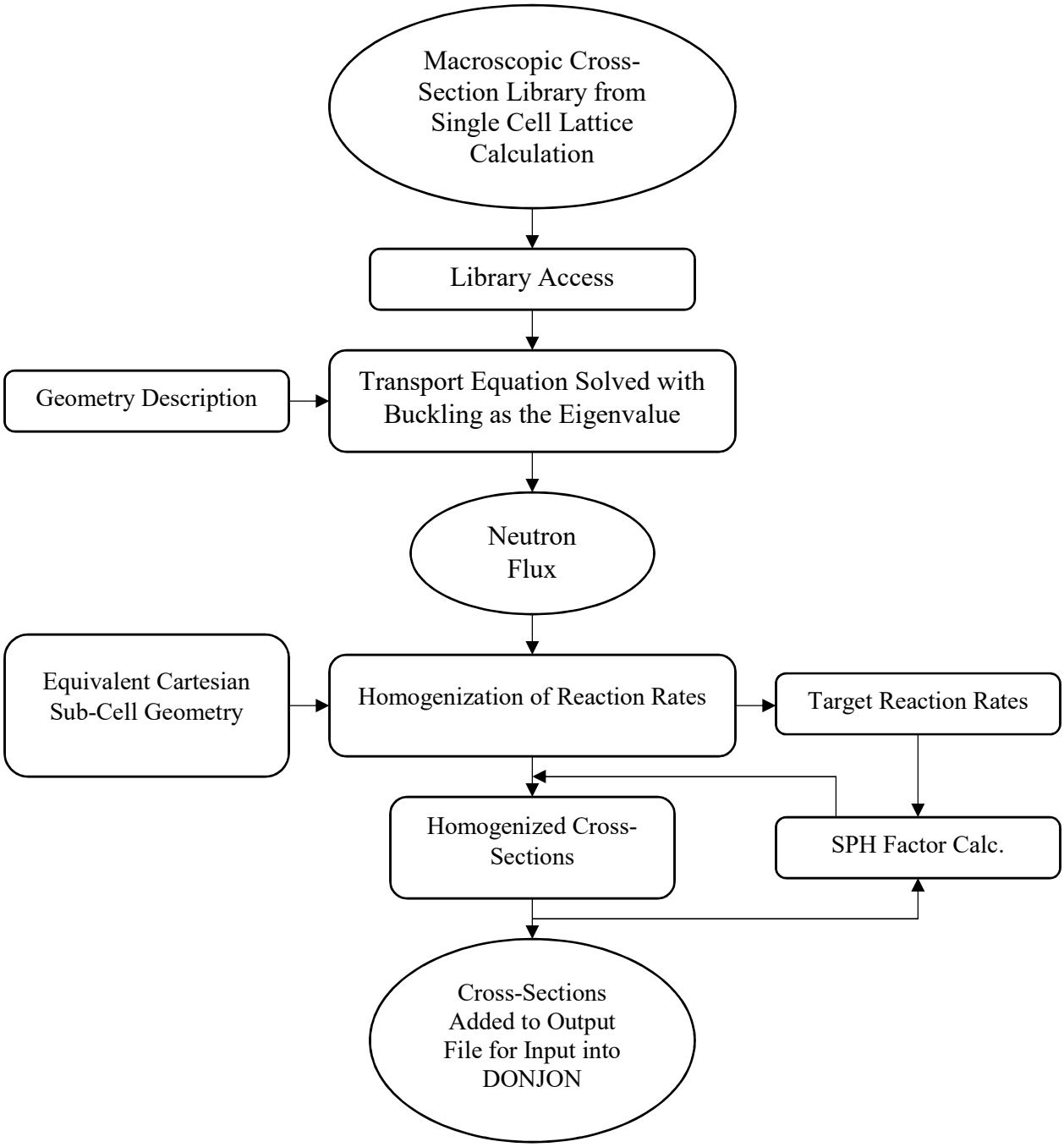

Figure 4.6: The Data flow in DRAGON for sub-cell homogenization with SPH factors for the multi-cell lattice calculation.

4.1.3. Single-Cell Diffusion Models

The aim of this study was to compare lattice level results from a detailed transport calculation to the lattice level results for the homogenized diffusion calculation. The diffusion lattice cell model used for core calculations in DONJON was generated to give an equivalent 3×3 sub-divided cell. A standard homogenized lattice cell was also created for comparison both of which are shown in Figure 4.7 below.

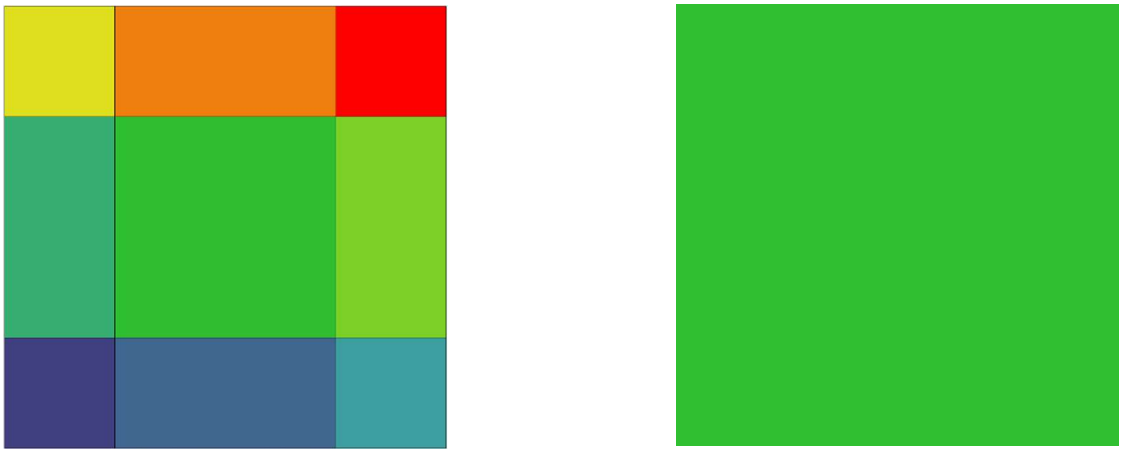

Figure 4.7: The two diffusion lattice cells. The left is the heterogenous cell and the right is the homogenous lattice cell.

4.2. Reference and Core Calculation Models

Multiple 5×5 partial core models were developed to asses the performance of SPH factors with improved boundary conditions. There were six different configurations of fresh fuel and discharge fuel partial core models and an additional checkboard voided coolant core were developed. Reflective boundary conditions were used for all calculations. DRAGON was used to generate reference results against which the SPH method was compared. The DONJON diffusion code was used to perform all

homogenous core calculations. Multiple diffusion cores were modelled for each fuel burnup configuration for each of the different lattice cell homogenization calculations. One for standard homogenization from a single lattice cell, another for standard homogenization for a partial core lattice calculation. Additional two for sub-cell homogenization with SPH factors from both single cell and partial core lattice calculations.

4.2.1. Detailed Reference Transport Models

A detailed transport partial core model was developed for each fuel burnup combination as a reference for both fission rate and multiplication constant in DRAGON. A total of 7 reference models were developed, each containing 25 lattice cells assembled into a 5×5 square. The lattice cells all have the same spatial discretization as the single bundle lattice cell discussed in Section 4.1, each consisting of 179 regions for a total of 4475 regions. All models use the 2 energy group cross-sections generated from the single bundle calculation. Figures 4.8 to 4.12 depict the fuel burnup combinations used. All bundles were modelled to have discharge burnup unless denoted by ZB (zero burnup), which were modelled as fresh fuel. The first evaluated configuration consisted of three fresh fuel bundles and is shown in Figure 4.8 below.

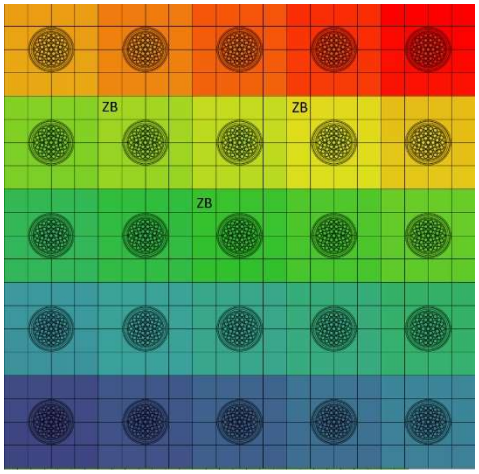

Figure 4.8: 5×5 reference core model with three fresh fuel bundles.

Partial cores with four fresh fuel bundles were subsequently evaluated and are depicted in the following Figure 4.9.

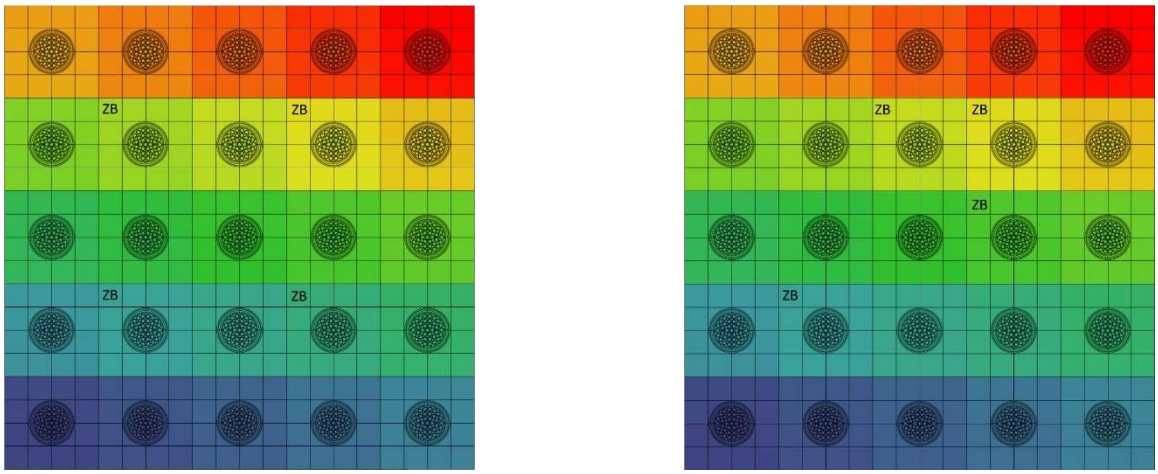

a) b)

Figure 4.9: 5×5 reference core models with four fresh fuel bundles.

Followed by the evaluation with five fresh fuel bundles as shown in Figure 4.10.

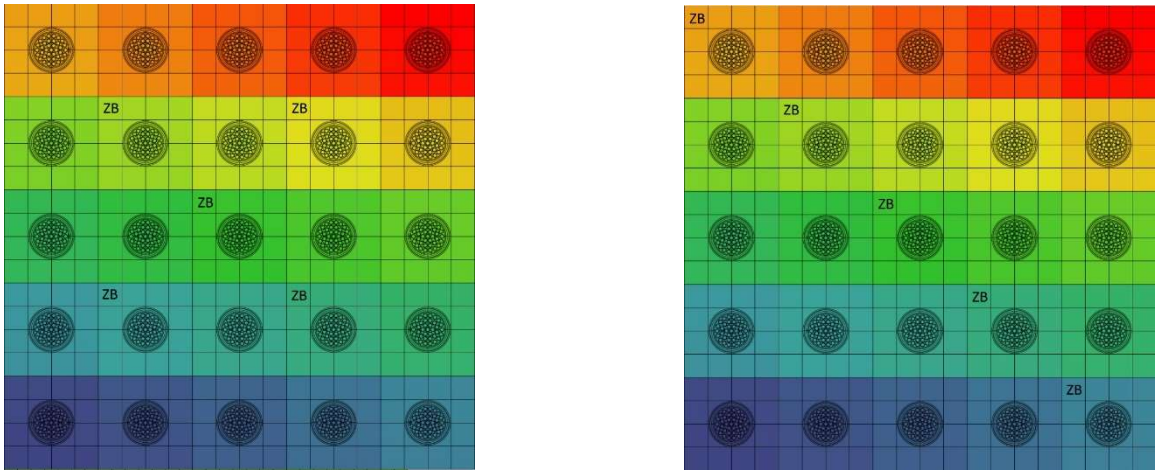

a) b)

Figure 4.10: 5×5 reference core models with five fresh fuel bundles.

Finally, a partial core with six fresh fuel bundles was evaluated as depicted in Figure 4.11.

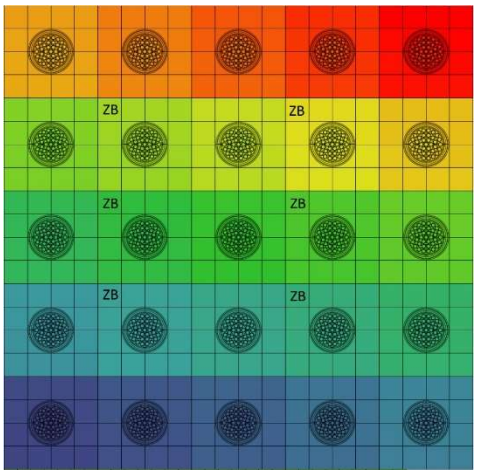

Figure 4.11: 5×5 reference core models with six fresh fuel bundles.

To simulate the effectiveness of the SPH method's ability to asses Loss of Coolant Accidents (LOCA), a partial core with a checkerboard pattern of lattice cells with voided

coolant was developed and shown in Figure 4.12. The lattice cells with voided coolant are indicated by a V and all fuel bundles were modeled with a discharge burnup level.

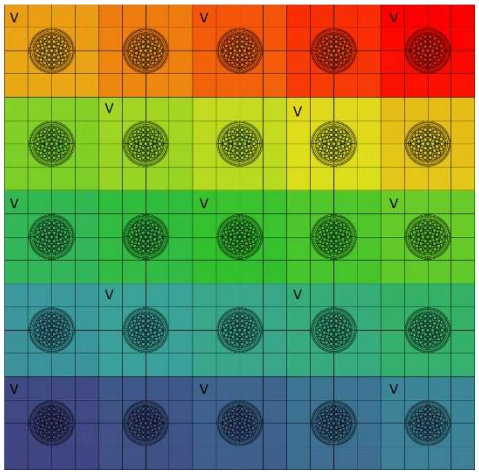

Figure 4.12: 5×5 reference core model with a voided coolant fuel bundles.

4.2.2. Partial-Core Diffusion Models

The diffusion 5×5 cores that were modelled in DONJON consisted of heterogeneous diffusion lattice cells with 9 sub-cell divisions, or a single homogenized lattice cells as described in Section 4.1.3. There were 7 different partial core configurations developed to match the configurations of the reference partial cores that were being simulated. All configurations were repeated for each lattice cell homogenization approach that was being evaluated.

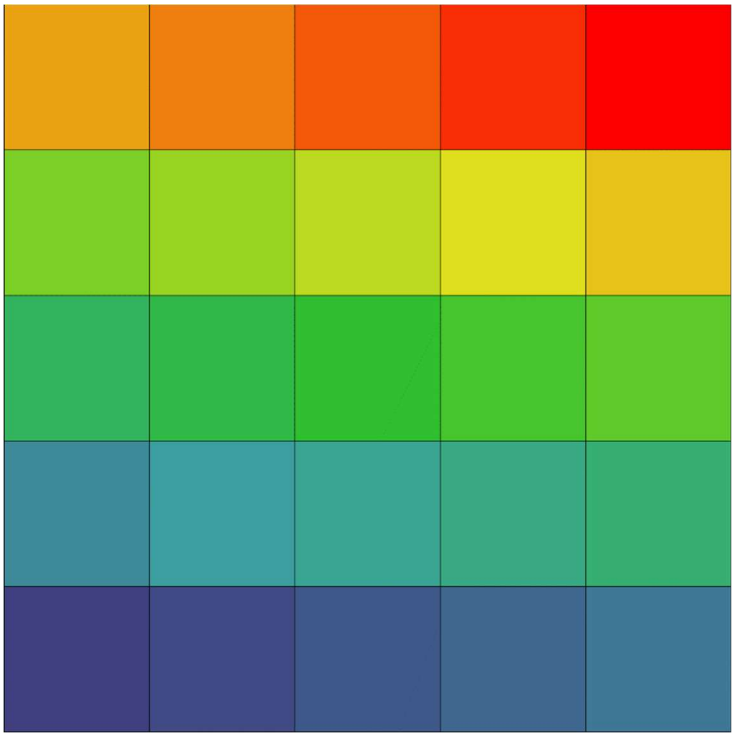

Figure 4.13: 5×5 homogenous diffusion core model.

Figure 4.13 above depicts the homogenized diffusion core that was used for all seven fuel channel configurations that were assessed. All reactor cores consist of 25 regions. Figure 4.14 below portrays the equivalent heterogenous diffusion model that consists of the sub-divided lattice cell and each consist of 225 regions.

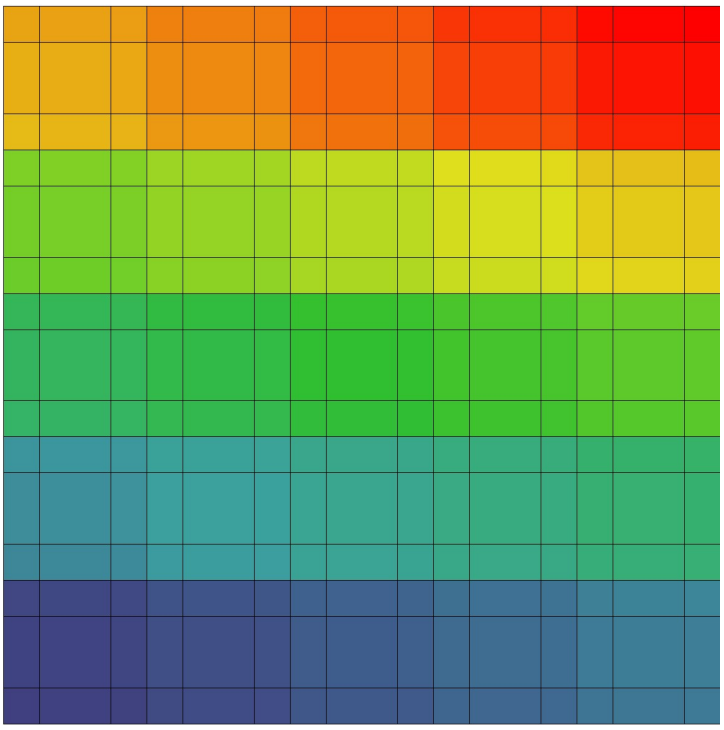

Figure 4.14: 5×5 homogenous diffusion core model.

Chapter 5: Results and Discussion

5.1. Reaction Rate Normalization

For multiplying media, both the transport equation and the diffusion equations are eigenvalue problems, where the neutron flux is the eigenfunction and the multiplication constant is the eigenvalue. As a result, the neutron flux can only be determined up to a multiplicative constant, requiring some normalization procedure for comparison between the two solutions. In this thesis, reaction rate normalization will be applied, such that there is a reaction rate of 1 fission per second in each lattice cell.

The total reaction rate (RR) for a reactor is given in Eq. (5.1), where C is the number of lattice cells defined by region, R, where V_{rc} is the volume of a sub-region, r, within the cell. The macroscopic fission cross-section is given as $\Sigma_{f,grc}$, for energy group g and sub region r in lattice cell c, and $\bar{\phi}_{grc}$ is the normalized flux for group g and region r of lattice cell c.

$$RR_T = \sum_{c=1}^{C} \sum_{r=1}^{R} V_{rc} \left(\sum_{g=1}^{G} (\Sigma_{f,grc} \times \bar{\phi}_{grc} \right) \tag{5.1}$$

The normalized flux is determined from the average flux, ϕ_{grc}, of region r, group g, and cell c, and a normalization constant A, as shown in Eq. (5.2).

$$\bar{\phi}_{grc} = A\phi_{grc} \tag{5.2}$$

Since A is a constant and can be factored out of the summations. Eq. (5.1) can be written as follows:

$$RR_T = A \sum_{c=1}^{C} \sum_{r=1}^{R} V_{rc} \left(\sum_{g=1}^{G} (\Sigma_{f,grc} \times \phi_{grc} \right) \tag{5.3}$$

The above expression can then be written to solve for the normalization constant.

$$A = \frac{RR_T}{\sum_{c=1}^{C}\sum_{r=1}^{R} V_{rc}(\sum_{g=1}^{G}(\Sigma_{f,grc}\times\phi_{grc})} \quad (5.4)$$

The value for RR_T, is always equal to the number of lattice cells (25) in this work. Once the normalization constant has been solved the normalized flux can be determined from Eq. (5.2).

5.2. Results

The 5×5 core DRAGON results (k_{eff}, fluxes, reaction rates) are taken as reference and all DONJON results will be compared to them. The evaluation of the diffusion core is done by assessing the percent difference in the bundle fission rates (FR) and the difference in k_{eff}. The percent difference is calculated using Eq. (5.5), and the difference in k_{eff} is calculated using Eq. (5.6), where FR_{DRAGON} and FR_{DONJON} are the normalized fission rates from the DRAGON reference calculation and the DONJON calculation respectively.

$$\%diff_{FR} = \frac{FR_{DONJON}-FR_{DRAGON}}{FR_{DRAGON}} \times 100\% \quad (5.5)$$

$$diff_{k-eff} = k_{eff,DONJON} - k_{eff,DRAGON} \quad (5.6)$$

For all fuel burnup configurations, the results for the four lattice calculation approaches were compared; single-cell standard homogenization (SC-SH), single-cell sub-cell homogenization with SPH factors (SC-SPH), multi-cell standard homogenization (MC-SH), and multi-cell sub-cell homogenization with SPH factors (MC-SPH). Tables 5.1-5.7 show the results for each of the 5×5 full-core configurations, which differ only in the arrangement of the fresh-fuel cells. The top row shows k_{eff} results, while the bottom five rows show fission-rate results for the 5x5 configuration. In each table cell, the top box shows the reference transport calculation result, while the four boxes below show the

difference between the homogenized-model results and the reference (transport) results for each of the four homogenization approaches. Cells corresponding to fresh fuel are shaded and the numbers are shown in bold.

Table 5.1: Comparison of k_{eff} and normalized reaction rates for the core depicted in Figure 4.8.

k_{eff} (DRG)	0.9882				
k_{eff} difference (SC-SH)	-0.0232				
k_{eff} difference (SC-SPH)	-0.0231				
k_{eff} difference (MC-SH)	0.0005				
k_{eff} difference (MC-SPH)	0.0005				
FR (DRG)	1.0012	1.0131	1.0153	1.0131	1.0012
%diff(SC-SH)	1.35	2.92	3.23	2.92	1.35
%diff (SC-SPH)	1.00	2.71	2.94	2.73	1.03
%diff (MC-SH)	1.19	2.26	2.39	2.26	1.19
%diff (MC-SPH)	2.78	2.11	4.16	2.11	2.78
	1.0018	**1.1369**	1.0298	**1.1369**	1.0018
	1.55	**5.96**	5.18	**5.96**	1.55
	1.31	**8.02**	5.17	**8.06**	1.36
	1.32	**2.71**	3.61	**2.71**	1.31
	1.21	**2.13**	3.09	**2.13**	1.21
	0.9821	1.0023	**1.1286**	1.0023	0.9821
	-0.87	1.82	**5.16**	1.82	-0.87
	-1.27	1.66	**7.23**	1.80	-1.21
	-0.37	1.37	**2.05**	1.37	-0.37
	0.35	0.90	**2.25**	0.90	0.35
	0.9578	0.9666	0.9748	0.9666	0.9578
	-4.05	-2.80	-1.70	-2.80	-4.05
	-4.55	-3.24	-1.96	-3.04	-4.50
	-2.50	-1.73	-1.00	-1.73	-2.50
	-3.02	-1.56	-1.42	-1.56	-3.02
	0.9431	0.9465	0.9488	0.9465	0.9431
	-6.04	-5.54	-5.21	-5.54	-6.04
	-6.62	-6.08	-5.71	-6.06	-6.58
	-3.87	-3.54	-3.32	-3.54	-3.87
	-4.34	-4.01	-3.78	-4.01	-4.34

Table 5.2: Comparison of k_{eff} and normalized reaction rates for the core depicted in Figure 4.9 a).

k_{eff} (DRG)	0.9926				
k_{eff} difference (SC-SH)	-0.0238				
k_{eff} difference (SC-SPH)	-0.0235				
k_{eff} difference (MC-SH)	-0.0003				
k_{eff} difference (MC-SPH)	-0.0000				
FR (DRG)	0.9690	0.9783	0.9787	0.9783	0.9690
%diff(SC-SH)	-2.04	-0.83	-0.76	-0.83	-2.05
%diff (SC-SPH)	-2.53	-1.20	-1.23	-1.20	-2.54
%diff (MC-SH)	-1.11	-0.27	-0.30	-0.27	-1.11
%diff (MC-SPH)	0.33	-0.53	1.31	-0.53	0.33
	0.9783	**1.1041**	0.9934	**1.1041**	0.9783
	-0.83	**2.72**	1.11	**2.72**	-0.83
	-1.20	**4.56**	0.85	**4.56**	-1.20
	-0.27	**0.67**	0.99	**0.67**	-0.28
	-0.53	**-0.75**	0.23	**-0.75**	-0.53
	0.9788	0.9934	0.9927	0.9934	0.9788
	-0.76	1.11	1.05	1.11	-0.76
	-1.23	0.84	0.59	0.84	-1.23
	-0.31	0.98	0.84	0.98	-0.31
	1.32	0.24	2.32	0.24	1.32
	0.9783	**1.1041**	0.9934	**1.1041**	0.9783
	-0.84	**2.71**	1.11	**2.71**	-0.84
	-1.20	**4.56**	0.84	**4.56**	-1.21
	-0.28	**0.66**	0.98	**0.66**	-0.28
	-0.51	**-0.73**	0.26	**-0.73**	-0.51
	0.9690	0.9783	0.9788	0.9783	0.9690
	-2.05	-0.84	-0.76	-0.84	-2.05
	-2.54	-1.20	-1.23	-1.21	-2.54
	-1.12	-0.28	-0.29	-0.29	-1.12
	0.36	-0.49	-1.19	-0.49	0.36

Table 5.3: Comparison of k_{eff} and normalized reaction rates for the core depicted in Figure 4.9 b).

k_{eff} (DRG)	0.9931				
k_{eff} difference (SC-SH)	-0.0220				
k_{eff} difference (SC-SPH)	-0.0227				
k_{eff} difference (MC-SH)	0.0006				
k_{eff} difference (MC-SPH)	-0.0004				
FR (DRG)	0.9541	0.9721	0.9997	1.0091	0.9990
%diff(SC-SH)	-5.29	-2.11	2.34	4.01	2.78
%diff (SC-SPH)	-5.88	-2.62	2.03	3.75	2.40
%diff (MC-SH)	-2.41	-0.85	1.61	2.35	1.50
%diff (MC-SPH)	-3.01	-0.12	1.54	3.63	3.07
	0.9615	0.9814	**1.1321**	**1.1463**	1.0073
	-5.17	-0.95	**6.83**	**8.95**	4.19
	-5.73	-1.31	**8.89**	**11.17**	3.93
	-1.77	-0.00	**2.77**	**3.87**	2.21
	-2.36	-0.54	**2.40**	**2.72**	3.48
	0.9789	0.9799	1.0005	**1.1274**	0.9945
	-5.80	-0.62	3.78	**7.27**	2.88
	-6.36	-1.03	3.52	**9.34**	2.57
	-0.37	-0.23	1.60	**2.44**	1.11
	-0.95	0.37	1.95	**2.07**	2.45
	1.1062	**0.9745**	0.9679	0.9706	0.9625
	-16.23	**12.15**	0.61	0.16	-1.14
	-16.65	**14.03**	0.19	-0.21	-1.64
	0.60	**-0.72**	-1.21	-0.93	-1.67
	-1.12	**-1.28**	-1.10	-1.40	-0.88
	0.9781	0.9612	0.9495	0.9445	0.9412
	-7.38	-3.60	-2.89	-3.46	-4.00
	-7.96	-4.07	-3.46	-4.03	-4.59
	-0.55	-1.96	-2.86	-3.27	-3.57
	-0.39	-1.24	-3.43	-3.78	-4.06

Table 5.4: Comparison of k_{eff} and normalized reaction rates for the core depicted in Figure 4.10 a).

k_{eff} (DRG)	0.9976				
k_{eff} difference (SC-SH)	-0.0214				
k_{eff} difference (SC-SPH)	-0.0210				
k_{eff} difference (MC-SH)	-0.0004				
k_{eff} difference (MC-SPH)	-0.0002				
FR (DRG)	0.9573	0.9694	0.9718	0.9694	0.9573
%diff(SC-SH)	-3.15	-1.54	-1.20	-1.54	-3.15
%diff (SC-SPH)	-3.76	-2.03	-1.77	-2.03	-3.77
%diff (MC-SH)	-1.76	-0.65	-0.50	-0.65	-1.76
%diff (MC-SPH)	-0.55	-1.12	0.91	-1.12	-0.55
	0.9694	**1.1019**	0.9989	**1.1019**	0.9694
	-1.55	**2.97**	2.33	**2.97**	-1.55
	-2.03	**4.69**	2.03	**4.69**	-2.03
	-0.66	**0.87**	1.82	**0.86**	-0.66
	-1.12	**-0.06**	0.97	**-0.06**	-1.12
	0.9719	0.9989	**1.1243**	0.9989	0.9719
	-1.20	2.33	**5.63**	2.33	-1.20
	-1.78	2.03	**7.39**	2.03	-1.78
	-0.50	1.82	**2.41**	1.82	-0.50
	0.91	0.97	**3.23**	0.97	0.90
	0.9694	**1.1020**	0.9989	**1.1020**	0.9694
	-1.55	**2.97**	2.33	**2.97**	-1.55
	-2.03	**4.69**	2.03	**4.69**	-2.03
	-0.66	**0.86**	1.82	**0.86**	-0.66
	-1.12	**-0.06**	0.97	**-0.06**	-1.12
	0.9574	0.9694	0.9719	0.9694	0.9574
	-3.16	-1.55	-1.20	-1.55	-3.16
	-3.77	-2.03	-1.78	-2.03	-3.77
	-1.76	-0.66	-0.50	-0.66	-1.76
	-0.55	-1.12	0.90	-1.12	-0.55

Table 5.5: Comparison of k_{eff} and normalized reaction rates for the core depicted in Figure 4.10 b).

k_{eff} (DRG)	0.9983				
k_{eff} difference (SC-SH)	-0.0200				
k_{eff} difference (SC-SPH)	-0.0196				
k_{eff} difference (MC-SH)	0.0008				
k_{eff} difference (MC-SPH)	0.0009				
FR (DRG)	**1.1751**	1.0140	0.9658	0.9337	0.9180
%diff(SC-SH)	**11.80**	4.36	-2.15	-6.58	-8.77
%diff (SC-SPH)	**13.98**	4.05	-2.76	-7.33	-9.60
%diff (MC-SH)	**6.35**	3.16	-1.07	-3.91	-5.43
%diff (MC-SPH)	**6.24**	3.28	-0.22	-4.43	-5.90
	1.0140	**1.1192**	0.9804	0.9495	0.9337
	4.36	**4.86**	-0.37	-4.44	-6.58
	4.05	**6.63**	-0.79	-5.13	-7.33
	3.16	**2.07**	0.14	-2.54	-3.91
	3.28	**2.21**	-0.23	-2.36	-4.43
	0.9658	0.9804	**1.1004**	0.9804	0.9658
	-2.15	-0.37	**2.40**	-0.37	-2.15
	-2.77	-0.80	**4.05**	-0.80	-2.77
	-1.04	0.14	**0.51**	0.14	-1.04
	-0.22	-0.23	**0.67**	-0.24	-0.22
	0.9337	0.9495	0.9804	**1.1193**	1.0141
	-6.58	-4.45	-0.37	**4.86**	4.35
	-7.33	-5.13	-0.80	**6.62**	4.04
	-3.91	-2.55	0.14	**2.07**	3.16
	-4.43	-2.37	-0.24	**2.21**	3.28
	0.9180	0.9338	0.9658	1.0141	**1.1751**
	-8.78	-6.59	-2.16	4.35	**11.79**
	-9.60	-7.33	-2.77	4.04	**13.97**
	-5.43	-3.92	-1.04	3.16	**6.34**
	-5.90	-4.43	-0.22	3.27	**6.23**

Table 5.6: Comparison of k_{eff} and normalized reaction rates for the core depicted in Figure 4.11.

k_{eff} (DRG)	1.0025				
k_{eff} difference (SC-SH)	-0.0199				
k_{eff} difference (SC-SPH)	-0.0194				
k_{eff} difference (MC-SH)	0.0005				
k_{eff} difference (MC-SPH)	-0.0001				
FR (DRG)	0.9487	0.9598	0.9611	0.9598	0.9487
%diff(SC-SH)	-3.84	-2.35	-2.18	2.35	3.84
%diff (SC-SPH)	-4.57	-2.94	-2.88	2.94	4.57
%diff (MC-SH)	-2.12	-1.10	-1.06	1.10	2.12
%diff (MC-SPH)	-1.07	-1.72	0.17	1.72	1.07
	0.9677	**1.1002**	0.9895	**1.1002**	0.9677
	-1.28	**3.26**	1.59	**3.26**	-1.28
	-1.88	**4.95**	1.07	**4.95**	-1.88
	-0.47	**1.14**	1.37	**1.14**	-0.47
	0.23	**-0.62**	1.52	**-0.62**	0.23
	0.9775	**1.1171**	1.0035	**1.1171**	0.9775
	0.03	**5.26**	3.42	**5.26**	0.03
	-0.56	**7.06**	2.88	**7.06**	-0.56
	0.32	**2.38**	2.48	**2.38**	0.32
	2.15	**0.64**	3.61	**0.64**	2.14
	0.9677	**1.1003**	0.9896	**1.1003**	0.9677
	-1.28	**3.26**	1.59	**3.26**	-1.28
	-1.88	**4.95**	1.07	**4.94**	-1.88
	-0.47	**1.14**	1.37	**1.14**	-0.47
	0.22	**-0.63**	1.52	**-0.63**	0.22
	0.9487	0.9598	0.9612	0.9599	0.9487
	-3.84	-2.35	-2.18	-2.35	-3.84
	-4.57	-2.95	-2.88	-2.95	-4.57
	-2.13	-1.11	-1.07	-1.11	-2.13
	-1.08	-1.72	0.16	-1.73	-1.08

Table 5.7: Comparison of k_{eff} and normalized reaction rates for the core depicted in Figure 4.12.

k_{eff} (DRG)	0.9803				
k_{eff} difference (SC-SH)	-0.0278				
k_{eff} difference (SC-SPH)	-0.0280				
k_{eff} difference (MC-SH)	0.0004				
k_{eff} difference (MC-SPH)	0.0003				
FR (DRG)	**1.0222**	0.9767	**1.0214**	0.9767	**1.0222**
%diff(SC-SH)	**-0.20**	0.29	**-0.27**	0.29	**-0.20**
%diff (SC-SPH)	**-0.30**	0.42	**-0.38**	0.42	**-0.30**
%diff (MC-SH)	**-0.14**	0.14	**-0.10**	0.14	**-0.13**
%diff (MC-SPH)	**0.30**	-0.21	**0.19**	-0.21	**0.30**
	0.9767	**1.0214**	0.9763	**1.0214**	0.9767
	0.29	**-0.27**	0.27	**-0.27**	0.29
	0.42	**-0.38**	0.40	**-0.39**	0.42
	0.14	**-0.09**	0.10	**-0.09**	0.14
	-0.21	**0.02**	-0.09	**0.02**	-0.21
	1.0214	0.9763	**1.0212**	0.9763	**1.0214**
	-0.27	0.27	**-0.28**	0.27	**-0.27**
	-0.38	0.40	**-0.40**	0.40	**-0.38**
	-0.10	0.10	**-0.11**	0.10	**-0.10**
	0.18	-0.09	**0.01**	-0.09	**0.18**
	0.9767	**1.0214**	0.9763	**1.0214**	0.9767
	0.29	**-0.27**	0.27	**-0.27**	0.29
	0.42	**-0.39**	0.39	**-0.39**	0.42
	0.13	**-0.09**	0.10	**-0.09**	0.13
	-0.22	**0.02**	-0.09	**0.02**	-0.22
	1.0222	0.9767	**1.0214**	0.9767	**1.0222**
	-0.21	0.29	**-0.27**	0.29	**-0.21**
	-0.31	0.41	**-0.39**	0.41	**-0.31**
	-0.14	0.13	**-0.11**	0.13	**-0.14**
	0.29	-0.22	**0.18**	-0.22	**0.29**

For completion purposes, all lattice cell calculation approaches were compared in such a way as to simulate a Loss of Coolant Accident (LOCA). In a PHWR adjacent fuel channels have coolant flowing in opposite directions, and to simulate a LOCA for PHWRs bundles with voided coolant must be in an alternating checkboard pattern. The results for the calculations are presented in Table 5.7 above, where all bolded and shaded

sections represent coolant voided lattice cell. All bundles where at a discharge fuel burnup level.

5.3. Discussion

The results shown in Section 5.2 show that using a multi-cell model for homogenizing cross-section data greatly improves the accuracy of the homogenization compared to using a single cell model. Furthermore, when a single cell model is used, the use of SPH factors does not improve the results compared to standard homogenization, a result that agrees with the results found in the preceding study (Mohapatra, 2016). That study hypothesized that the reason for the lack of improvement may be due to errors in calculated SPH factors resulting from their dependence on inter-lattice cell leakage. This study accounted for inter-cell leakage by utilizing the multi-cell lattice calculation approach, and the SPH factor improvement for the multi-cell approach in comparison to the single cell approach can be seen in Table 5.8. The Figure 5.1 depicts which cell in the 5×5 core was used for comparison, and the regions within the cell that correspond to the SPH factor comparisons in Table 5.8.

Table 5.8: SPH factor comparison of the centre cell of the 5×5 core with diagonal orientation of fresh fuel.

	1	2	3
SPH Fact. (5×5)	0.912	0.945	0.934
% diff. (3×3)	7.84	7.54	6.90
% diff. (1×1)	10.77	9.63	8.06
	4	5	6
	0.945	0.841	0.967
	7.54	7.25	6.59
	9.63	7.44	7.21
	7	8	9
	0.934	0.967	0.947
	6.90	6.59	5.94
	8.06	7.21	6.66

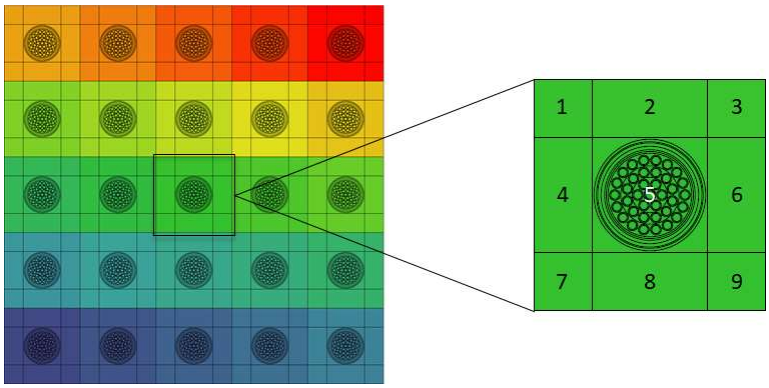

Figure 5.1: The cell and sub-regions corresponding to the SPH factor comparison in Table 5.8.

However, even with the improvement of the SPH factors, there is no better diffusion-transport reaction rate equivalence for sub-cell homogenization with SPH factors then

standard homogenization for a multi-cell lattice calculation step approach. In fact, the difference is almost identical as seen for the comparison for the single cell lattice calculation step. The SPH method as applied to LWRs in literature also demonstrated the improvement of the method with better boundary condition considerations (Hébert & Benoist, 1991 & Hébert, 1993). However, there was no comparison to the results of standard homogenization for the equivalent conditions.

A possible explanation as to why there is no improvement from sub-cell homogenization with SPH factors is the spatial discretization of the lattice cell is not fine enough to have significant improvement over standard homogenization. The largest region of heterogeneity is within in the fuel channel, which was not sub-divided in this study. However, due to the concentric ring design of the PHWR fuel bundle, further sub-cell homogenization in DRAGON is not possible and a different transport code would be required for further testing.

Another possible explanation is that the sub-cell homogenization improves the flux distribution within the cell but has little effect of the course cell-to-cell flux variation. The SPH factor normalization condition that was used in this study was the flux-volume condition, which ensures the spatially integrated macro-calculation (diffusion) flux for each group is equivalent to the transport model. However, the short coming of this approach is the flux continuity is not guaranteed between neighboring lattice cells in the diffusion calculation. The Selengut normalization condition was developed to ensure flux continuity between two lattice cells (Selengut, 1960). The Selengut methodology utilizes a normalization factor such that the surface fluxes are equal to one. There are two approaches for this method, the first uses the full cell averaged flux with the surface flux

of the transport calculation. The second approach uses the average flux of the water gap in the diffusion lattice cell and the surface flux of the transport calculation (Chambon & Hébert, 2015). Utilizing this different SPH normalization condition may improve the results by ensuring the continuity of the flux across cell borders and creating a better core flux shape.

However, both explanations provided above are not suspected to have considerable improvement on the results presented in this study. The difficulty that arises from the homogenization process is preserving all the parameters of the heterogenous model. The homogenous model, however, does not offer enough degrees of freedom (DOF) to be able to preserve all desired parameters (Smith, 1986). There are $G \times (N + 1)$ homogenous parameters, where G is the number of energy groups and $(N + 1)$ is the number of reaction types and the diffusion coefficient. However, there are $G \times (N + 2 \times D)$ parameters to be conserved, $G \times N$ reaction rates and $G \times 2 \times D$ currents for each surface of the region being homogenized, where D is the dimensions of the region being modelled. The SPH factors generated for sub-cell homogenization only add an additional G degrees of freedom and not enough to overcome the preservation problem (Berman, 2013). The Selengut normalization is not predicted to overcome this limitation, since the methodology is based on the average boundary flux and has not discrepancy between the fluxes on each surface of the lattice cell. As result, it does not add any additional degrees of freedom then the standard normalization approach.

Chapter 6: Summary, Conclusion, and Future Investigations

6.1. Summary and Conclusion

Previous work (Mohapatra, 2016) performed in an attempt to improve homogenization methods for PHWRs using sub-cell homogenization with Superhomogenization (SPH) equivalence factors was found to be unsuccessful. The reason for the lack of improvement was hypothesised to be due to SPH factors being dependent on inter-cell neutron leakage (NIchita & Mohapatra, 2016). Due to the ease of implementation of the SPH method into already established production reactor-physics simulation codes, there was interest in expanding the previous investigative work to improve SPH-homogenization results. In this thesis, SPH factors are calculated accounting for inter-cell leakage with the aim of improving homogenization results. Results for several homogenization approximations are compared: single-cell standard homogenization, single-cell SPH, multi-cell standard homogenization and multi-cell SPH.

The results for all calculations are shown is section 5.2 show that the most substantial improvement comes from the use of multi-cell lattice calculations, be they standard homogenization or SPH, with or without sub-region divisions. There is no significant improvement, or often even worse results from the use of sub-cell homogenization with SPH factors in comparison to standard homogenization. The multi-cell SPH approach is shown to improve the accuracy of calculated bundle powers compared to the single-cell SPH approach. However, the accuracy is comparable to the multi-cell standard homogenization approach as shown in Table 6.1.

Table 6.1: Summary of all methods and cores evaluated presented as root mean square (RMS) percent errors.

Number of Fresh Bundles	SC-SH RMS(%)	SC-SPH RMS (%)	MC-SH RMS (%)	MC-SPH RMS (%)
3	3.95	4.62	2.38	2.64
4a	1.62	2.41	0.70	0.83
4b	6.17	6.91	2.03	2.29
5a	2.57	3.39	1.26	1.11
5b	5.88	6.81	3.36	3.47
6	3.00	3.95	1.47	1.34
CB	0.27	0.39	0.12	0.19

The results obtained using the SPH method and those obtained using standard homogenization are almost identical for both single-cell and multi-cell lattice calculation approaches. The sub-cell homogenization with SPH factors may improve the accuracy of the power and neutron flux shapes within the cell, but not the bundle power and flux at the core level. That is because, as explained in Chapter 5, SPH factors do not provide sufficient degrees of freedom to preserve both the sub-region reaction rates and the inter-cell leakage rates; the latter being what determines the flux shape at the core level.

6.2. Future Investigations

Given that the utility of SPH factors is primarily in helping reproduce the power distribution within the cell, future work is warranted for this purpose. To achieve this goal, sub-regions need to correspond to individual fuel pins. Due to the geometry constraints of the DRAGON-code version utilized in this research, further splitting of the central sub-region (the ones containing the fuel) was not possible. Further work could be done to improve the pin-power distribution by utilizing finer sub-cell division in a

different transport code. Additionally, because only standard flux-volume normalization of the SPH factors (which does not ensure continuity of the flux at the inter-lattice cell boundary) was used in this thesis, further investigations may use different SPH factor normalization conditions such as one or all the different Selengut normalization conditions. However, because, as discussed in Chapter 5, such normalizations rely on using average cell boundary flux or current, they are only expected to yield improvements for cases in which all neighbours of a given cell are identical, such as in the case of checkerboard configurations, whereby either the burnup or the void fraction alternate between neighboring cells in a checkerboard pattern.

References

1. Aragonés, J. M., & Ahnert, C. (1986). A linear discontinuous finite difference formulation for synthetic coarse-mesh few-group diffusion calculations. *Nuclear Science and Engineering*, *94*(4), 309-322.
2. Auger, P., Munn, A. M., & Pontecorvo, B. (1947). The transport mean free path of thermal neutrons in heavy water. *Canadian journal of research*, *25*(3), 143-156.
3. Berman, Y. (2013). An improved homogenization technique for pin-by-pin diffusion calculations. *Annals of Nuclear Energy*, *53*, 238-243.
4. Chambon, R., & Hébert, A. (2015). A new open-source pin power reconstruction capability in DRAGON5 and DONJON5 neutronic codes. *Nuclear Engineering and Design*, *289*, 208-217.
5. Hebert, A. (1980). *Développement de la méthode SPH: Homogénéisation de cellules dans un réseau non uniforme et calcul des parametres de réflecteur* (Doctoral dissertation). UniversitÉ de Paris-Sud.
6. Hebert, A. (1993). A consistent technique for the pin-by-pin homogenization of a pressurized water reactor assembly. *Nuclear Science and Engineering*, *113*(3), 227-238.
7. Hébert, A. (2009). *Applied reactor physics*. Presses inter Polytechnique.
8. Hébert, A., & Benoist, P. (1991). A consistent technique for the global homogenization of a pressurized water reactor assembly. *Nuclear Science and Engineering*, *109*(4), 360-372.

9. Herrero, J. J., García-Herranz, N., Cuervo, D., & Ahnert, C. (2012). Neighborhood-corrected interface discontinuity factors for multi-group pin-by-pin diffusion calculations for LWR. *Annals of Nuclear Energy*, *46*, 106-115.
10. Jonkmans, G. (2006). WIMS-AECL version 3.1 User's Manual. ISTP-05-5115, *IST Product, Protected COG RandD, Atomic Energy of Canada Ltd*.
11. Kavenoky, A., "The SPH homogenization method."
12. Kim, H. R., & Cho, N. Z. (1993). Global/local iterative methods for equivalent diffusion theory parameters in nodal calculation. *Annals of Nuclear Energy*, *20*(11), 767-783.
13. Marleau, G., Hébert, A., & Roy, R. (2007). A user guide for DRAGON Version 3.05E. *IGE-174, Ecole Polytechnique de Montréal, Institut de génie nucléaire Département de génie mécanique (Oct. 2007)*.
14. Mohapatra, S. (2016). *Investigation of sub-cell homogenization for PHWR lattice cells using superhomogenization factors* (master's Thesis). University of Ontario Institute of Technology, Oshawa, Canada.
15. Nichita, E. (2015). *Partial-cell homogenization progress report*. Kingston, Canada: Queens University.
16. Nichita, E., Mohapatra, S. (2016). Application of SPH factors to PHWR lattice homogenization. *TRANSACTIONS-AMERICAN NUCLEAR SOCIETY*, 114, 77-780.
17. Piro, M. H. A., Wassermann, F., Grundmann, S., Tensuda, B., Kim, S. J., Christon, M., Berndt, M., Nishimura, M., & Tropea, C. (2017). Fluid flow investigations within a 37 element CANDU fuel bundle supported by magnetic

resonance velocimetry and computational fluid dynamics. *International Journal of Heat and Fluid Flow*, *66*, 27-42.

18. Pomraning, G. C. (1967). Variational principle for eigenvalue equations. *Journal of Mathematical Physics*, *8*(1), 149-158.
19. Rahnema, F. (1989). Boundary condition perturbation theory for use in spatial homogenization methods. *Nuclear Science and Engineering*, *102*(2), 183-190.
20. Rahnema, F., & Nichita, E. M. (1997). Leakage corrected spatial (assembly) homogenization technique. *Annals of Nuclear Energy*, *24*(6), 477-488.
21. Robinson, R. C., and Tran, F. (1995). Calculation of homogenized Pickering NGS stainless steel adjuster rod neutron cross-sections using conservation of reaction rates. 16th Annual CNS conference, June 4 - 7, 1995, Saskatoon, SK, Canada.
22. Sanchez, R., & McCormick, N. J. (1982). A review of neutron transport approximations. *Nuclear Science and Engineering*, *80*(4), 481-535.
23. Selengut, D.S., (1960). Diffusion coefficients for heterogenous systems. *TRANSACTIONS-AMERICAN NUCLEAR SOCIETY*, 3, 398.
24. Smith, K. S. (1980). *Spatial homogenization methods for light water reactor analysis* (Doctoral dissertation, Massachusetts Institute of Technology).
25. Smith, K. S. (1986). Assembly homogenization techniques for light water reactor analysis. *Progress in Nuclear Energy*, *17*(3), 303-335.
26. Varin, E., Hébert, A., Roy, R., & Koclas, J. (2005). A User Guide for DONJON Version 3.01. *École Polytechnique de Montréal Montréal QC, Canada, Tech. Rep. IGE-208*.